Mechanical properties and constitutive models of shape memory alloy for structural engineering: A review

Ali Mohammadgholipour and AHM Muntasir Billah[iD]

Abstract
Shape Memory Alloys (SMAs) are an innovative material with the unique features of superelasticity and energy dissipation capabilities under extreme loads. Due to their unique features, they have a great potential to be employed in structural engineering applications under different conditions. However, in order to effectively use SMAs in civil engineering structures and model their behaviors accurately in Finite Element (FE) packages, it is crucial for structural engineers to comprehend the mechanical properties and cyclic behavior of different SMA compositions under varying loading conditions. While previous studies have focused mainly on the cyclic behavior of SMAs under tensile loading, it is important to evaluate their fatigue behavior under cyclic tension-compression loading for seismic applications. This literature review aims to discuss the current gaps in the existing literature on the behavior of SMA rebars under low-cycle fatigue (LCF). The review provides a comprehensive overview of the primary characteristics of SMAs, summarizes the mechanical properties of SMAs presented in the literature and the parameters that affect them, and critically evaluates the effects of cyclic loading and LCF on SMAs. The review also provides a summary of the different constitutive models of SMAs and compares their advantages and limitations, which helps structural engineers to employ an appropriate constitutive model for predicting the accurate behavior of SMAs in FE software.

1. Introduction

It is expected that reinforced concrete (RC) structures designed by current structural design standards undergo significant inelastic deformation in certain zones under cyclic loading to dissipate energy (Wang and Zhu, 2018). However, the design of structures in compliance with this design philosophy may lead to difficult-to-repair damage, large permanent inter-story drifts in buildings, and significant permanent deformation in bridges, causing substantial socio-economic costs and inconvenience (Marquis et al., 2017; Wang and Zhu, 2018; Zhao et al., 2009). Several innovative systems and technologies have emerged to resolve these issues in recent years. Shape memory alloys (SMA) are one of these cutting-edge technologies that are used as reinforcing rebar in RC structures and have drawn a lot of interest from researchers because of their unique and desired performance under extreme loading. SMA is a material capable of experiencing significant strains and recover its original shape without experiencing residual strains. Since SMAs have high energy dissipation capacities and superelastic properties, they are ideal for applications under extreme loading such as earthquake (Alam et al., 2007a; Asfaw and Ozbulut, 2021) and impact (Gholipour and Billah, 2022).

During seismic occurrences, a reinforced concrete (RC) member is exposed to severe tension-compression strain reversals in the critical zones, resulting in low-cycle fatigue (LCF) damage to reinforcing rebars (Tripathi et al., 2018). When a rebar is exposed to cyclic loading with a large strain amplitude, such as during an earthquake, it fails prematurely after a limited number of cycles (Aldabagh and Alam, 2021; Tripathi et al., 2018). The fatigue life is defined as the number of

Department of Civil Engineering, University of Calgary, Calgary, AB, Canada

Corresponding author:
AHM Muntasir Billah, Department of Civil Engineering, University of Calgary, 2500 University Drive, N.W., Calgary, AB T2N 1N4, Canada.
Email: muntasir.billah@ucalgary.ca

cycles required to fail a reinforcing rebar. It is interesting to note that observations from past earthquakes and experiments show that the buckling fracture of longitudinal rebar because of LCF is one of the common failure modes for flexural members (Aldabagh and Alam, 2021; Paul et al., 2014). Therefore, since the buckling and fracture of longitudinal rebars in RC elements lead to significant moment and strength degradation, many studies have been conducted on the effects of inelastic buckling on the LCF behavior of reinforcing steel (Aldabagh and Alam, 2021; Kashani et al., 2015a, 2015b; Tripathi et al., 2018; Wu et al., 2022).

Due to the possible use of SMAs in various structural engineering applications, it is necessary for structural engineers to comprehend the inelastic cyclic behavior of different compositions of SMA rebar under varying loading conditions. This will facilitate selecting the optimal compositions depending on their demands and to properly simulate the SMA rebar response in Finite Element (FE) packages. Several studies have been conducted on the mechanical properties and the cyclic behavior of different compositions of SMAs (DesRoches et al., 2004; Dolce and Cardone, 2001; Fang et al., 2021; Hong et al., 2022; Wang and Zhu, 2018). Although, as mentioned, the buckling fracture of rebar is one of the most common failure modes, previous studies have mainly focused on the cyclic behavior of SMA rebars under tensile loadings. However, for seismic application of SMAs, their cyclic behavior and fatigue resistance under cyclic tension-compression loading conditions is crucial. This is because seismic loads have an intrinsic sinusoidal loading nature. Additionally, effect of strain rates is another important aspect, that needs to be investigated when SMA rebars are exposed to repeated tension-compression loading.

This literature review attempts to identify the current gaps in existing literature in regard to the behavior of SMA rebars under LCF, investigate the fatigue life of SMAs considering the effect of inelastic buckling, parameters that affect the cyclic response of SMA rebar, constitutive models of SMA rebar and finally identify the research needs for the SMA application in the seismic and vibration control of various types of civil engineering structures. To achieve these, this review provides a concise overview of the primary characteristics of SMAs, summarized existing information from literatures using useful tables and figures on the mechanical properties of SMAs, and a critical evaluation of the effects of cyclic loading and LCF on SMAs. This article also provides a concise summary of the different constitutive models of SMAs. This review is not intended to provide a detailed overview of applications of SMA in structural engineering, rather to summarize the behavior of various SMA compositions under cyclic tension-compression loading.

2. Shape memory alloys

The breakthrough in material science has pushed structural engineers to make structures that are adaptive and smart. It has also made researchers and structural engineers more excited to introduce innovative and smart materials in civil engineering structures (Alam et al., 2007b). Shape Memory Alloy (SMA) is a smart material that has received the interest of structural engineers and researchers due to its unique thermomechanical properties and flag-shaped hysteresis curve. SMAs have unique features, to recover their original shape when heated (Shape Memory Effect (SME)) and revert to their pristine state after removing loading (superelasticity (SE)) (Billah et al., 2022). Due to their high energy absorbing capabilities and significant reduction in residual deformation, SMAs are becoming a viable substitute for conventional steel (Alam et al., 2007b; Billah et al., 2022).

2.1. Shape memory effect (SME)

The shape memory effect (SME) is defined as the capability of a material to recover its original shape when heated. The shape memory effect was first observed in gold-cadmium (Au-Cd) in 1932 through metallographic observations and resistivity changes (Ölander, 1932). Buehler and Wiley (1961) combined Nickel and Titanium to develop alloys showing the SME. Several alloys with shape memory effect have been presented in recent years, the most common of which are nickel-titanium SMAs (Ni-Ti) (Buehler and Wiley, 1961; Dolce and Cardone, 2001; Frick et al., 2004), copper-based SMAs (Cu-SMAs) (Araki et al., 2011; Zhang et al., 2009), and iron-based SMAs (Czaderski et al., 2014; Ghafoori et al., 2017; Tanaka et al., 2010). SMAs can be in two different states: austenite and martensite. Austenite happens at high temperatures, while martensite happens at low temperatures (Alam et al., 2007b). The phase transformation between two phases is shown in Figure 1(a). SMAs are characterized by four distinct transformation temperature, which are the martensite start temperature (M_s), martensite finish temperature (M_f), austenite start temperature (A_s), and austenite finish temperature (A_f). SMAs have multiple crystal structures that possess the same chemical compositions. Chemical composition and thermomechanical processing control the dominant crystal structure, which depends on stress and temperature (Dolce and Cardone, 2001). According to Figure 1(a) and (b), when the temperature is lower than the Austenite start temperature $(T < A_s)$, and the SMA experiences large deformation under loading, the SMA will maintain some of the permanent strain following unloading. When the deformed specimen is heated above the austenite start temperature (A_s), the phase transformation from martensite to austenite begins. The transformation
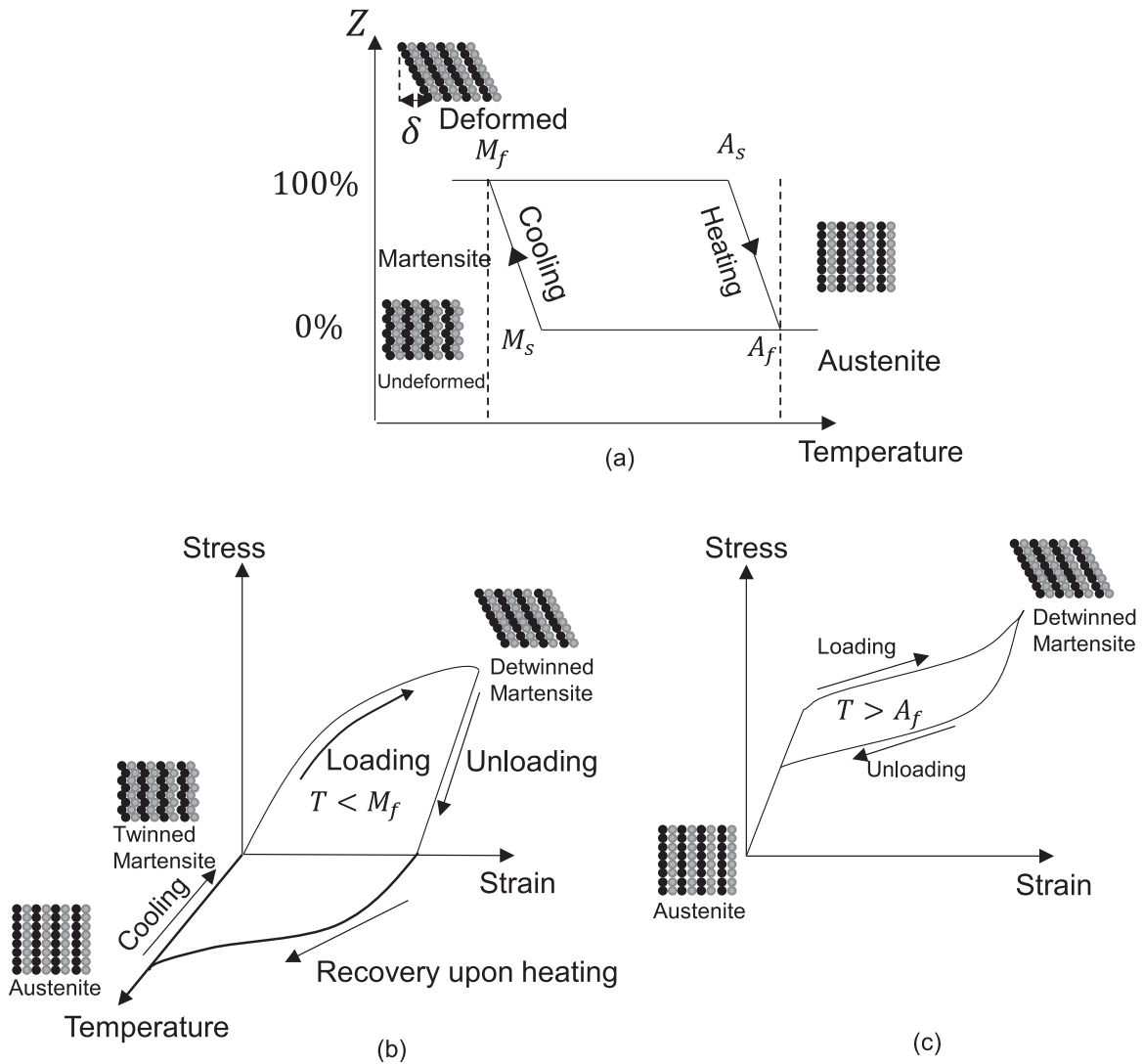
Figure 1. Cyclic behavior of SMAs: (a) phase transformation between austenite and martensite, (b) shape memory behavior of SMAs, and (c) superelastic behavior of SMAs.

phase will be completed at A_f $(T>A_f)$, and the SMA will revert to its original shape. This is defined as the shape memory effect. SMA is fully in the martensite phase and austenite phase when the temperature is lower than M_f $(T<M_f)$ and higher than A_f $(T>A_f)$. It should be noted that a small change in the composition of SMAs can affect the transformation temperatures (Abdulridha, 2013; Alam et al., 2007b).

2.2. Superelasticity effect (SE)

The ability of a material to recover its original shape after being loaded is referred to as the superelasticity effect (SE). SMAs show superelastic behavior at temperatures higher than austenite finish temperature $(T>A_f)$. Figure 1(c) shows the superelasticity effect. As can be seen, upon loading, after a certain stress level, the SMA goes into the martensite phase. However, after unloading, the martensite becomes unstable, and

the SMA recovers its original shape. This capability of SMAs is considered an advantage in structural engineering applications since it would be capable of recovering displacement under dynamic loading (Abdulridha, 2013; Alam et al., 2007b).

3. SMA compositions

There have been several compositions of SMAs developed in recent years. Among them Ni-Ti SMAs gained substantial interest because of their exceptional recovery strain and corrosion resistance. However, large-scale practical applications were impossible due to high production costs and difficult machining processes (Billah et al., 2022). The high cost of production prompted researchers to seek out superior substitute compositions exhibiting desired superelastic and shape-memory properties. In recent years, different

Table 1. Different compositions of SMAs.

SMA alloy	Reference	Compositions (%)	M_f(°C)	M_s(°C)	A_s(°C)	A_f(°C)
Ni-Ti	Hesse et al. (2004)	55.7 44.3	−40.15	4.85	17.85	50.85
Cu-Zn-Al	Vivet and Lexcellent (2001)	25.63 4.2 70.17	15.35	19.5	20.05	25.15
Cu-Al-Be	Rejzner et al. (2002)	25.6 4.2 70.2	−116.5	−94.5	−104.15	−78.15
Cu-Al-Ni	Recarte et al. (2004)	82 14 4	−21.5	−27.5	0.85	11.85
Cu-Al-Mn	Shrestha et al. (2013)	71.7 16.7 11.6	−91	−74	−54	−39
Fe-Mn-Si-Cr-Ni-1(V,C)	Lee et al. (2015)	64 17 5 10 4	−64	−60	103	162
Fe-Ni-Co-Ti	Tanaka et al. (2010)	43.5 28 17 11.5	—	—	—	—
Fe-Mn-Al-Ni	Vollmer et al. (2021)	44.4 32.8 15.2 7.6	—	—	—	—

Figure 2. The bibliography mapping of SMAs.

composition of shape memory alloys (Cu-based (Cu-Zn-Al, Cu-Al-Be, Cu-Al-Ni, Cu-Al-Mn) and Fe-based (Fe-Mn-Si-Cr-Ni-1(V,C), Fe-Ni-Co-Ti, Fe-Mn-Si)) have been developed as viable alternatives due to their low production costs and straightforward manufacturing procedures (Billah et al., 2022). Different compositions of SMAs, suitable for civil engineering applications, are presented in Table 1.

The commercial availability of different composition of SMAs in market vary depending on the specific requirements and applications. The most common composition of SMA is Ni-Ti, which is known as Nitinol. This composition is widely available in different forms (wire, ribbon, sheet, and bar) from several manufacturers; however, wire is the most common form available in market. Cu-based SMAs (Cu-Zn-Al, Cu-Al-Be, Cu-Al-Ni, and Cu-Al-Mn) and Fe-based (Fe-Mn-Si-Cr-Ni-1(V,C), Fe-Ni-Co-Ti, and Fe-Mn-Al-Ni) SMAs are also commercially available. However, there are very few suppliers and manufacturers of Cu and Fe SMAs compared to Ni-Ti SMA. Because of the popularity and application of Ni-Ti SMA in different industries such as biomedical and automobile, Ni-Ti is commercially more available than Cu and Fe SMA.

4. Structural engineering applications of SMA

SMAs' superelastic and shape memory properties made them appealing for civil engineering applications aimed at reducing structural damage. The review of the civil engineering application of SMAs was studied by many researchers (Alam et al., 2007b; Billah et al., 2022; DesRoches and Smith, 2004; Dong et al., 2011; Ozbulut et al., 2011; Song et al., 2006; Wilson and Wesolowsky, 2005). The bibliography mapping of SMAs is shown in Figure 2. Many researchers have studied the use of Shape Memory Alloys in various structures such as isolators, dampers, and new constructions, including reinforcement in concrete, bolted joints, bracings, prestressing, and restrainers (Alam et al., 2007b). The studies mostly focused on the

Table 2. The effects of SMA rebars on reinforced concrete members.

Reference	Application	Type	Size (mm)	Results
Ayoub (2003)	Concrete beam	Rebar	9.53 and 12.7	SMA reduced the residual strain by more than 75%
Saiidi et al. (2007)	Concrete beam	Rebar	9.53 and 12.7	SMA reduced the residual strain by more than 80%
Saiidi and Wang (2006)	Concrete column	Rebar	12.7	SMA recovered nearly all of the post yield deformation
Saiidi et al. (2009)	Concrete bridge column	Rebar	12.7	SMA reduced the residual strain by more than 80%
Youssef et al. (2008)	Concrete beam-column joint	Rebar	20.6	SMA reduced the residual beam rotation by 50%
Alam et al. (2007c)	Concrete beam-column joint	Rebar	20.6	SMA recovered most of the post-yield deformation
Nahar et al. (2019)	Concrete beam-column joint	Rebar	8, 20, 24, and 28	SMA rebars decreased the energy dissipation capacity of the RC bram-column joints rather than regular steel rebar; however, they recover most of the post yield deformation.
Hoult and de Almeida(2022)	Concrete shear wall	Rebar	12.7	SMA rebars concentrated strain at the base of the RC wall in contrast to steel rebar.
Abraik et al. (2020)	Concrete shear wall	Rebar	15 and 25	SMA rebars reduced the residual displacement by 36%, and the diaphragm rotation by 6% to 58%
Abdulridha and Palermo (2017)	Concrete shear wall	Rebar	12.7 and 16	The hybrid SMA reinforced concrete wall and steel rebar reinforced concrete shear wall recovers 92% and 31% of residual strain, respectively.

superelasticity and shape memory effects of SMAs, and they found that the use of SMAs in structures would allow structures to remain serviceable with no or little damage under extreme loading conditions. Due to Ni-Ti SMAs' favorable mechanical properties, they are more widely utilized as rebars in civil engineering structures than other types of SMAs (Billah et al., 2022). Therefore, this section discusses the usage of Ni-Ti shape memory alloy (SMA) rebars in concrete structures.

Several studies have examined the use of SMA rebars in concrete members. Table 2 presents a summary of experimental studies on the effects of Ni-Ti SMA rebars in concrete members. Ayoub (2003) assessed the superelastic behavior of Ni-Ti SMA reinforcing bars in concrete beams subjected to half-cycle loadings. The results revealed that the average residual strain for SMA RC beams was around 75% of that for conventional steel RC beams, despite the fact that SMA-reinforced beams were less stiff than steel-reinforced beams. Saiidi et al. (2007) studied experimentally the application of SMA rebar in a concrete beam and observed that SMA rebars minimize residual strain by around 80%. In another experimental study, Saiidi and Wang (2006) used SMA rebars in the plastic hinge area of a concrete column to reduce the residual strain. The results showed that the after yielding, distortion of the SMA RC column was almost fully recovered.

Abraik et al. (2020) investigated the seismic performance of concrete core walls reinforced with Ni-Ti SMA rebars in terms of residual displacement, floor acceleration, and residual in-plane rotation. They concluded that the SMA RC wall experienced lower floor accelerations, residual displacements, and residual in plane rotation than concrete wall reinforced with steel rebar. Abdulridha and Palermo (2017) studied the effectiveness of a slender concrete wall reinforced with the combination of steel rebars and Ni-Ti rebars. The results revealed that the concrete wall reinforced with the combination of SMA and steel rebars recovers 92% of residual strain, while the concrete wall reinforced with steel rebars recovered 31% of residual strain. Hoult and de Almeida (2022) investigated the use of shape memory alloys in reducing residual displacements of RC walls during earthquakes. They found that in comparison to the steel RC wall, the SMA specimen concentrates the strain at the base of the RC wall at different strain amplitudes, and the specimen detailed with shape memory alloys had an equivalent plastic hinge length that was almost constant throughout the drift range. The results of this study provided insight into crack distributions, longitudinal strain profiles, and curvature profiles for structural engineers.

Saiidi et al. (2009) assessed the use of Ni-Ti SMA rebar in RC columns subjected to quasi-static cyclic loading. They discovered that SMA decreased the residual strain by over 80%. Youssef et al. (2008) examined the application of Ni-Ti SMA rebar in RC beam-column joints and found that the SMA rebar reduced permanent beam rotation by 50%. The SMA also significantly reduced the residual story drift. Alam et al. (2007c) studied the behavior of SMA-reinforced beam-column joints under reverse cyclic loading. The

behavior of the two specimens under reverse cyclic loading was compared based on load-story drift, moment-rotation envelope relationship, and energy dissipation ability. The results indicated that the SMA-reinforced beam-column specimen was able to regain the majority of its deformation after yielding. Nahar et al. (2019) investigated the seismic behavior of RC beam-column joints. They compared the effects of five different types of SMAs and steel rebar on the seismic behavior of joints and the performance was assessed based on load versus story drifts, residual strain, and cumulative energy dissipation capacity. They concluded that among different compositions of SMA rebar, Fe-Mn-Al-Ni rebar showed more desirable performance.

Furthermore, several studies have examined the application of SMAs in large-scale concrete structures. Siddiquee et al. (2021) assessed the seismic performance of 3-, 6-, and 8-story concrete buildings reinforced with Ni-Ti SMA rebar. In this study, they assessed the Collapse Margin Ratio (CMR), which is calculated as the ratio of ground motion intensity at the median collapse point to the ground motion intensity of the Maximum Considered Earthquake (MCE) at the building's fundamental period. Four different types of reinforcement detailing were considered. The results showed that the application of SMA rebars increased the collapse capacity of 3- and 8-story RC buildings. Rahman and Billah (2020) compared the seismic responses of bridge bents reinforced with SMA rebars and steel rebars under long duration ground motions. They considered different arrangements for reinforcement detailing. They found that SMA reinforced bents showed more desired performance than steel reinforced bents. They also discovered that the application of SMA rebar in the plastic hinge region improved the collapse behavior under the long-duration motions.

According to prior research, SMAs perform effectively in civil engineering structures and should be utilized in civil engineering applications to limit the damage caused by unforeseen events, such as earthquakes (Saiidi et al., 2007). Billah and Alam (2016a) developed damage states for the performance based seismic design of five SMA RC bridge piers under different seismic hazard scenarios. They also proposed a correlation between maximum drift, residual drift, and superelastic strain of SMA to predict the residual drift of bridge piers. Billah and Alam (2016b) evaluated the effects of different parameters on the plastic hinge length of concrete piers reinforced with SMA rebars and proposed a model to predict the potential plastic hinge length. The accuracy of the proposed model was validated by experimental tests.

The purpose of this section was to provide a brief overview of the applications of SMAs and it is not intended to summarize the various applications of SMAs. To find out more about the applications of SMAs, several review papers have been focused on the
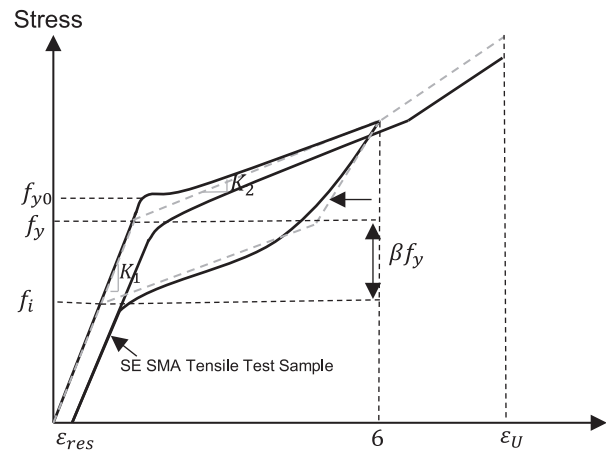

Figure 3. Tensile behavior of superelastic SMA material tested using ASTM F2516-07 (2007).

application of SMAs in civil engineering structures (Alam et al., 2007b; Billah et al., 2022; Dong et al., 2011; Ozbulut et al., 2011; Song et al., 2006).

5. Mechanical properties of SMA

Due to the desirable performance and distinctive characteristics of SMAs, structural engineers are interested in utilizing this material in civil engineering applications, particularly as reinforcing rebars in concrete members. However, no standard exists to characterize the mechanical properties of various SMA types under tension-compression loading for use in civil engineering applications (Tazarv and Saiid Saiidi, 2015). Regarding tensile testing of Ni-Ti superelastic SMA, there is just one standard, ASTM F2516-07 (2007), which was established for medical applications to measure upper plateau strength, lower plateau strength, residual strain, and tensile strength. Because the whole stress-strain model is necessary to simulate precisely the behavior of SMAs in civil engineering applications, and this cannot be developed with this limited data, these parameters do not adequately meet the interests of structural engineers.

Figure 3 illustrates the behavior of a superelastic SMA material evaluated according to ASTM F2516-07 (2007). As can be observed, the sample test consists of loading to 6% strain, unloading, and then loading to failure. In this figure, f_{y0} is defined as yield strength on the first cycle of loading, K_1 is the elastic modulus at austenite phase, which is the slope between 1.5% and 70% of f_{y0}, K_2 is the stiffness of the material after yielding, which is the average slope of the curve between 2.5% and 3.5% of strain on the upper plateau, f_i is the lower plateau inflection strength, $\beta = 1 - \frac{f_i}{f_y}$ is the lower plateau stress factor, ε_{res} is residual strain, $\varepsilon_r \leqslant 6\%$ is
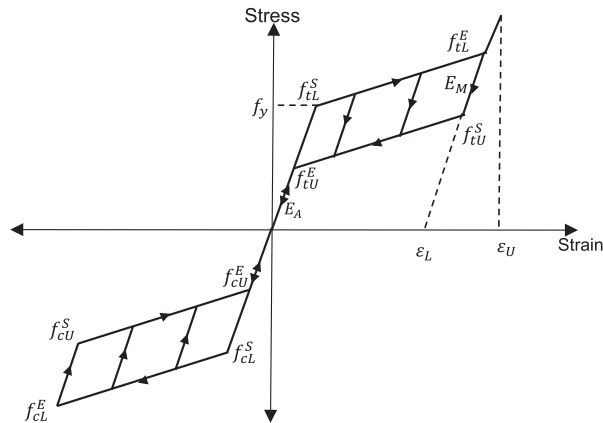
Figure 4. Tensile-compressive hysteretic behavior of SMAs.

recoverable superelastic strain, and ε_u is ultimate strain or strain at failure (ASTM F2516-07, 2007; Tazarv and Saiid Saiidi, 2015).

SMA exhibits a flag-shaped hysteretic response under tensile and compressive loads, as shown in Figure 4. The stress-strain curve starts with an elastic behavior up to the start transformation loading stress under tension (f_{tl}^S). Loading below the transformation strain shows superelastic behavior. After unloading within tension plateau region, the pass is a line with the slope of E_M, which is defined martensite elasticity modulus. The unloading pass continues with the loading pass slope in the transformation region until reaching end transformation unloading stress (f_{tl}^E), and then

returns to the origin with the slope of E_A. The compressive loading pass reaches start transformation loading under compression (f_{cl}^s) and completes a tension-compression cycle at F_{cl}^E, F_{cu}^S, and F_{cu}^E. The slope of compression plateau depends on the rebar slenderness, which may cause buckling under compression. This will be discussed further in the following sections.

As mentioned previously, some compositions of SMAs are appropriate for structural applications; however, structural engineers should consider the mechanical properties of different compositions of SMAs to choose the best one in accordance with their needs. Table 3 summarized the mechanical properties of different compositions of SMAs in literature. The properties include the tensile yield strength (f_{yt}), compressive yield strength (f_{yc}), austenite elastic modulus (E_A), and recovery strain (ε_l) as these are major material properties for SMAs.

Figure 5 shows the average tensile yield strength (f_{yt}) for the different compositions of SMAs. As shown, the mean f_{yt} for Fe-SMAs (Fe-Ni-Co-Al-Ta-B and Fe-Mn-Si-Cr-Ni-1(V,C)) is higher than other SMA compositions, while this value for the Cu-SMAs (Cu-Al-Mn and Cu-Al-Be) is the least. The mean tensile (f_{yt}) for Ni-Ti SMA rebar is about 400 MPa. It should be noted that as shown in Table 3, the f_{yc} for Ni-Ti SMAs was higher than f_{yt}.

Furthermore, austenite elastic modulus (E_A) is a parameter that represents the stiffness of the materials and how a material resists elastic deformations. Figure 6

Table 3. A summary of mechanical properties presented in the literature for different compositions of SMAs.

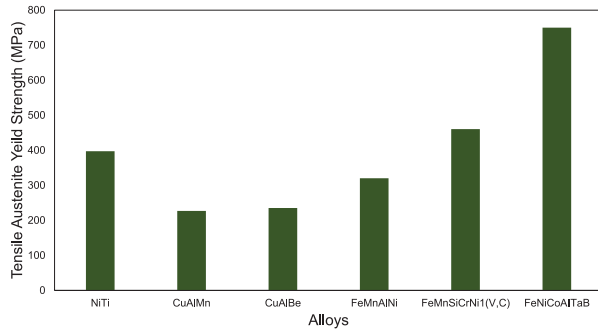| Alloys	Room temperature (°C)	F_{yt} (MPa)	F_{yc} (MPa)	E_A (GPa)	ε_l (%)	Reference
Ni-Ti	25	385	503	43	7.5	Frick et al. (2004)
	25	336	469	26	7.5	Frick et al. (2004)
	—	379	379	39.7	5.5	Alam et al. (2008)
	—	401	401	62.5	6	Alam et al. (2008)
	23–26	460.7	621.3	30.7	6	Wang and Zhu (2018)
	—	435	—	68	8	Ghassemieh et al. (2012)
	—	378	—	39.7	5.5	Saiidi and Wang (2006)
	—	401	—	62.5	6	Youssef et al. (2008)
	20–25	195–690	—	30	<8	DesRoches et al. (2004)
	—	383	—	28	6	McCormick and DesRoches (2006)
	—	414	—	27.5	6	McCormick and DesRoches (2006)
Cu-Al-Mn	—	210	—	33.9	—	Hosseini et al. (2015)
	20–25	160–180	—	20	12	Araki et al. (2011)
	20–25	260	—	20	9	Araki et al. (2011)
	—	210	—	28	9	Shrestha et al. (2013)
Cu-Al-Be	23	235	—	32.04	5	Zhang et al. (2009)
Fe-Mn-Al-Ni	—	320	—	98.4	6.13	Omori et al. (2011)
Fe-Mn-Si-Cr-Ni-1(V,C)	—	450	—	184	—	Rosa et al.(2021)
	23	310	—	200	1.15	Koster et al. (2015)
	25.5	546	—	173	1.3	Ghafoori et al. (2017)
	25	546	—	173	—	Hosseini et al. (2018)
	—	496–533	—	160	0.16–0.39	Shahverdi et al. (2018)
Fe-Ni-Co-Al-Ta-B	—	750	—	46.9	13.5	Tanaka et al. (2010)

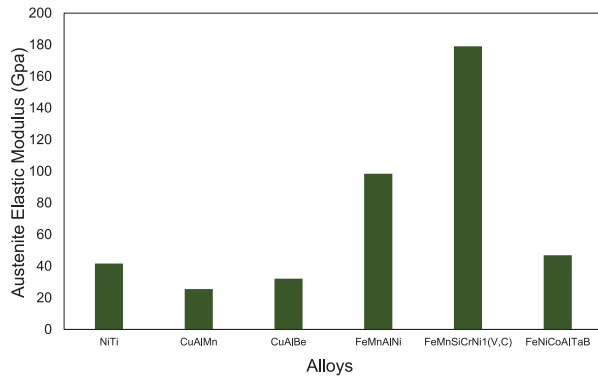**Figure 5.** The mean tensile yield strength for different compositions of SMAs.

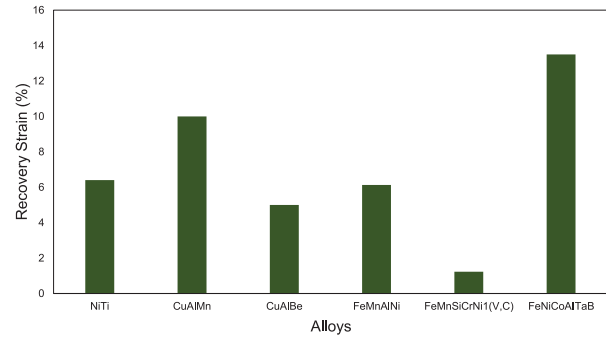**Figure 6.** The mean austenite elastic modulus for different compositions of SMAs.

Figure 7. The mean recovery strain for different compositions of SMAs.

SMA can be used as a good alternative for regular steel bars in RC bridge piers to minimize the damages caused by earthquakes.

6. Behavior of SMAs under cyclic loading

As previously mentioned, researchers in the earthquake and structural engineering fields have shown considerable interest in SMAs for enhancing the resilience of infrastructures due to their superelasticity and self-centering capabilities. Due to the fact that structural elements and materials experience large cyclic strain during seismic events, the self-centering characteristics of SMAs can withstand strong earthquakes. The elements can dissipate seismic energy while experiencing a large strain and recover their original shape without any residual strain. Therefore, it would be necessary to examine the LCF response of SMAs under reverse cyclic load to find their performance considering inelastic buckling. Several researchers examined the cyclic behavior of different types of SMAs and determined their mechanical properties and capability of energy dissipation in various conditions, such as different loading rates and temperatures, to comprehend the efficacy of SMAs in various applications related to civil engineering. Figure 8 compares the hysteretic curve of SMAs with different compositions (Cu SMAs, Fe SMAs, and Ni-Ti SMAs) at room temperature (Fang et al., 2021; Kato et al., 1999; Wang and Zhu, 2018). Cu-based SMAs and Ni-Ti-based SMAs exhibited a flag-shaped hysteretic curve, which validates the expected self-centering behavior of these SMA compositions, however the Fe-based SMAs do not exhibit a comparable curve (Fang et al., 2021; Kato et al., 1999; Wang and Zhu, 2018). The reason for this difference is the partial superelasticity of Fe-SMAs. Fang et al. (2021) studied experimentally the cyclic behavior of Fe SMAs under different strain amplitudes and found that the recovery strain for Fe SMAs is 5%–10% of the maximum strain amplitude at room temperature. It is also shown in Table 3 and Figure 7 that Fe SMAs have the lowest
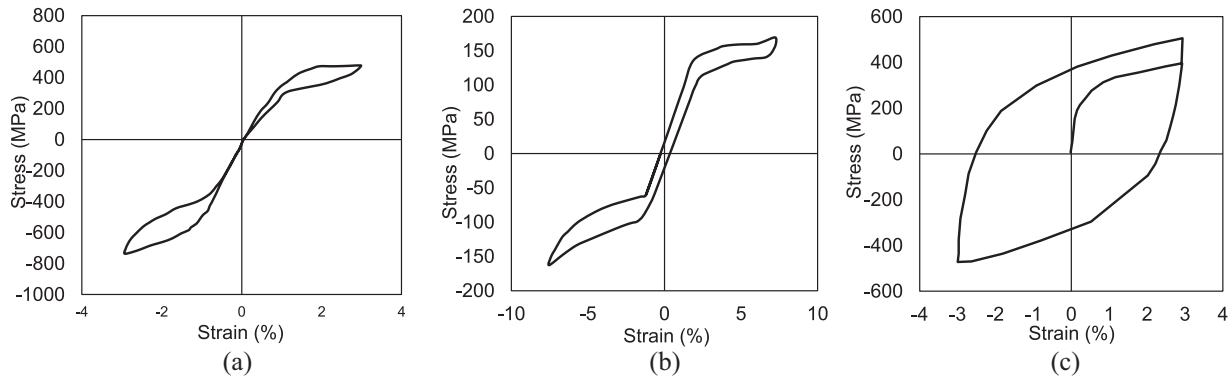
compares the average of E_A for different SMA compositions. As shown, the mean E_A for Fe-Mn-Si-Cr-Ni-1(V,C) SMA is much higher than Ni-Ti and Cu SMAs which are in the range between 30–68 GPa and 20–34 GPa, respectively. As a result, Fe-Mn-Si-Cr-Ni-1(V,C) would be stiffer than other compositions. It should be noted that Cu SMAs has the least elastic modulus (about 200 MPa). Figure 7 compares the recovery strain of different SMA compositions. According to Figure 7, Fe-Mn-Si-Cr-Ni-1(V,C) SMA shows the less superelasticity than other compositions since the recovery strain for this composition is about 2%, while this value for Fe-Ni-Co-Al-Ta-B is 13.5%. The recovery strains for Ni-Ti, Cu-Al-Mn, and Cu-Al-Be SMAs are 6%, 10%, and 5%, respectively. The recovery strain has a considerable importance since SMAs with a reasonable recovery strain, would show a desirable self-centering and superelastic behavior (Billah et al., 2022). Many researchers worked on the importance of the unique feature of SMAs (superelasticity and energy dissipation capacity) in civil engineering applications. For example, Shrestha et al. (2013) found that since the Cu-Al-Mn SMA has better recentering capabilities than other compositions of SMAs, and it would be appropriate to be used in isolation bearings and dampers. Hosseini et al. (2015) also suggested that the Cu-Al-Mn

Figure 8. Comparison of stress-strain curve of different compositions of SMAs: (a) Ni-Ti SMA (Wang and Zhu, 2018), (b) Cu-Al-Mn SMA (Kato et al., 1999), and (c) Fe-Mn-Si-Cr-Ni-1(V,C) SMA (Fang et al., 2021).
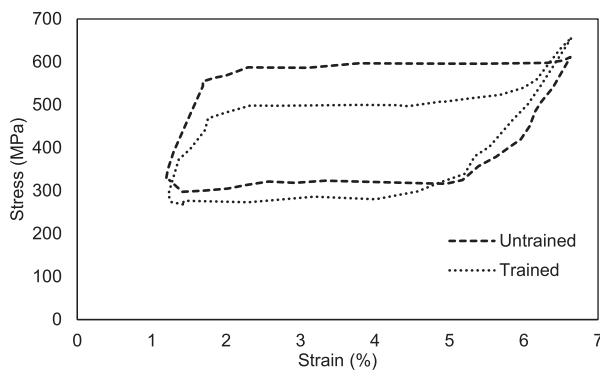

Figure 9. Comparison of trained and untrained SMA wire (Wolons et al., 1998).

value for recovery strain in comparison with other compositions, and subsequently a different hysteretic curve can be expected for the Fe SMAs. It is important to consider that although the superelastic behavior of Fe SMAs is less than other compositions, it has shown excellent shape-memory effect. In order to activate SME, Fe SMA must be heated to the temperature above A_f to recover the residual strain.

Furthermore, Wang and Zhu (2018) found the non-linear behavior of Ni-Ti SMA rebar is asymmetric under tension-compression cyclic loading. In other words, the value for compressive stress was more than that of tensile stress at the same strain level, and at high strain levels, the difference was significant (Wang and Zhu, 2018). According to Table 3, the compressive strength of Ni-Ti SMA is higher than its tensile stress. Liu et al. (1998) found that this asymmetric behavior is because of different deformation mechanisms in tension and compression modes. Rosa et al. (2021) indicated that there is an asymmetric stress-strain relationship between the tensile-compressive cyclic behavior of Ni-Ti SMAs, since the activation of the reverse transformation may occur at room temperature depending on the stress level under uniaxial compressive loading. The same behavior was observed in Cu SMAs of various

compositions. Kato et al. (1999) observed an asymmetric stress-strain curve for Cu-Al-Mn between tension and compression, and the area of the hysteretic loop under compressive loading was much larger than that under tensile loading. However, Fang et al. (2021) found that the hysteresis behavior of Fe-SMA is symmetric. The symmetric and asymmetric behavior of stress-strain curve for different compositions of SMAs can be observed in Figure 8. Therefore, according to the past studies, an asymmetric stress-strain curve can be expected for Cu and Ni-Ti SMAs, while the stress-strain behavior of Fe-SMA is symmetric when the cyclic behavior of SMAs is evaluated.

In the next section, the cyclic behavior of SMAs and the effects of training, different temperature, different loading rate, different diameters, and LCF on the hysteretic curve of SMAs with varied compositions have been discussed.

6.1. Training

Miyazaki (1990) suggested that superelastic SMAs should be trained before being tested under cyclic loading. The training process involves preloading SMA bars with relatively large strain amplitudes for several cycles. By doing this, steady-state hysteresis loops are obtained under cyclic tensile loadings without a change in transformation stress and permanent strain. Wolons et al. (1998) found that although each cycle of loading produces residual strain, it is the early cycles that produce the largest residual strains. Due to the residual strain that is developed in the first cycles, a significant amount of mechanical cyclic loading is needed to stabilize the SMA hysteresis loop shape. They also investigated the effects of cyclic loading on a trained and an untrained wire. They found that the phase of transformation plateau and the stress required to produce the unloading transformation for the trained wire was lower than that for the untrained wire. Figure 9 depicts the hysteretic loop of trained and untrained Ni-Ti
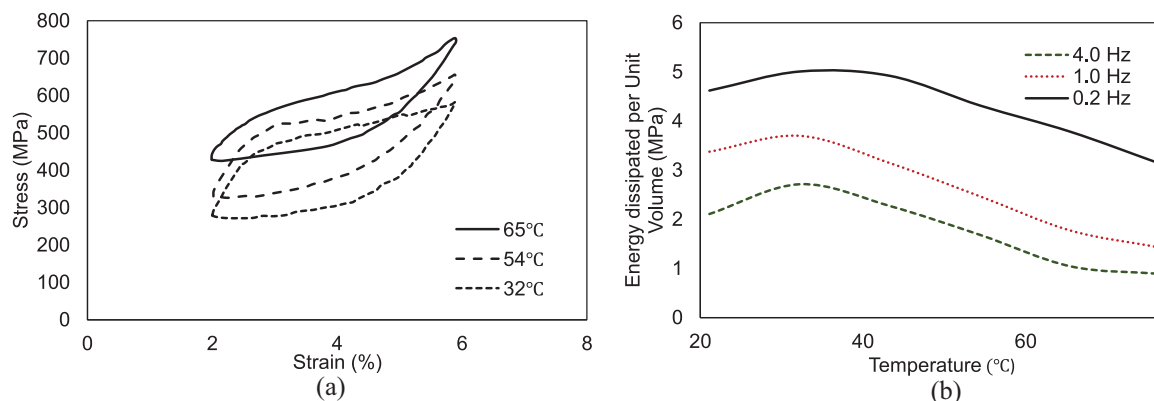
Figure 10. (a) Effects of temperature on the hysteresis loop of a Ni-Ti Wire and (b) effects of temperature and loading frequency on dissipated energy (Wolons et al., 1998).

SMA wire with the diameter of 0.5 mm. Because the hysteresis loop for a trained wire is smaller than for an untrained wire, the trained wire dissipated less energy. Therefore, it should be noted that, for damping applications where it is required to have large dissipating energy, the effects of training should be considered. It is noteworthy that if the SMA rebars are subjected to tension-compression cyclic loadings, training may not be necessary since, as a result of the reversed compression loading, the localized slip or dislocation formation in the martensite phase is suppressed and restored (Wang and Zhu, 2018).

6.2. Loading rate and temperature

To fully develop and exploit the potential of SMAs, a precise understanding of their behavior at different temperatures and strain loading rates is essential (Lee et al., 2013a). Due to its relevance to seismic applications, the impact of different strain loading rates and temperatures on the hysteretic curve of SMAs is crucial. The significance of these parameters stems from the fact that under extremely strong loading, the material's temperature rises and there is insufficient time for it to cool, which may influence the area of the stress-strain curve (Rosa et al., 2021). Therefore, in this section, the effects of various loading rates and temperatures are evaluated.

Wolons et al. (1998) investigated experimentally the cyclic behavior of 0.5 mm Ni-Ti SMA wires subjected to axial loading at various frequencies and temperatures. They discovered that the residual strain of Ni-Ti SMA wires is influenced by temperature and strain amplitude, but not strain loading rate. The hysteresis loop and dissipated energy of Ni-Ti SMAs were also found to be impacted by temperature and excitation frequency. As loading frequency increased beyond 0.1 Hz, the area of the hysteresis loop decreased due to a rise in unloading transformation stress. Figure 10(a) illustrates the temperature effects on 0.5 mm Ni-Ti

SMA wires. An increase in temperature also influenced the hysteresis curve of the Ni-Ti SMA and caused an upward move in the stress-strain curve. For a temperature higher than 32 °C, the area of hysteresis became smaller, and the amount of dissipated energy decreased. Figure 10(b) shows the effects of temperature and loading frequency on dissipated energy. As shown, the amount of dissipated energy decreased by 40% when temperature increased from 32 °C to 54 °C, and when loading frequency increased, the amount of dissipated energy decreased. Therefore, the amount of dissipated energy is dependent on loading frequency and temperature (Wolons et al., 1998).

Furthermore, Dolce and Cardone (2001) studied the effects of strain rate and temperature on the tensile cyclic behavior of superelastic Ni-Ti SMA wires with a diameter of 1–2 mm with respect to secant stiffness, energy loss per cycle, equivalent damping, and residual strain. The results demonstrated that an increase in strain loading rate from 0.02 to 0.2 Hz lowered the area of the hysteresis loop roughly by 18% and 25%, respectively. Loading frequency also influences the stress levels due to the upward movement of the hysteresis loop and the hardening of the phase transformation's branch. The secant elastic modulus increased by approximately 15% under the loadings with the frequency range between 0.02 and 0.2 Hz. They found that energy loss, equivalent damping, and secant stiffness of the Ni-Ti SMA wires are related to the loading rate frequency. They also found that temperature affects the mechanical properties of Ni-Ti SMA wires, however, the changes are lower than for other materials used in seismic applications. Thus, the Ni-Ti SMA wires are well suited for seismic applications (both self-centering and energy dissipation capabilities). DesRoches et al. (2004) assessed the influence of loading rates on the cyclic behavior of SMA wires and rebars under tensile loadings. The results showed that increasing the strain rate increased the forward and reverse transformation stresses, resulting in a reduction in the equivalent damping of Ni-Ti
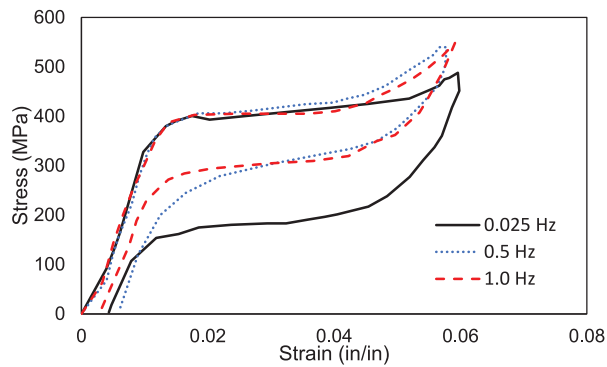
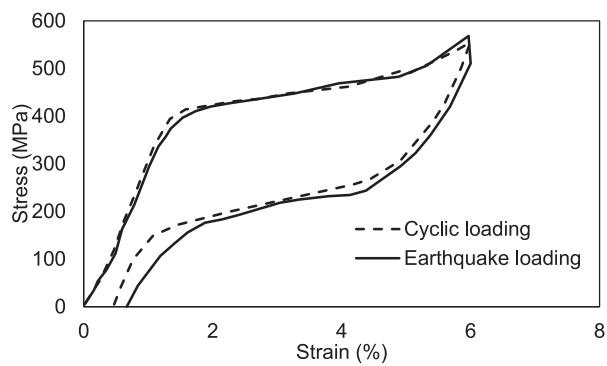**Figure 11.** Effects of loading frequency on the stress-strain curve of Ni-Ti SMA rebar (DesRoches et al., 2004).
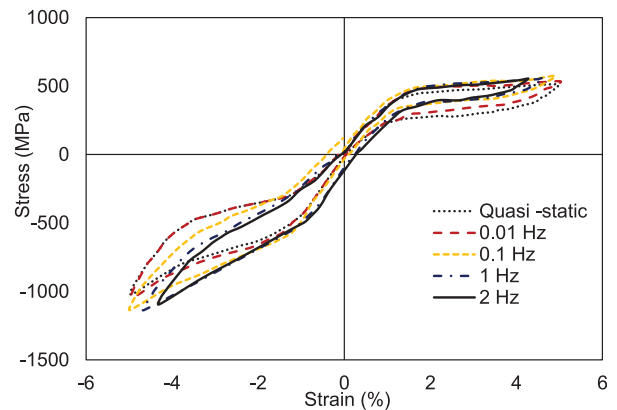

Figure 13. Loading frequency effect on the hysteresis curve of superelastic Ni-Ti SMA rebar with BRD (Wang and Zhu, 2018).

Figure 12. Stress-strain behavior of Ni-Ti SMA rebar with the diameter of 12.7 mm under earthquake and cyclic loading (McCormick et al., 2007).

different strain rates, strain amplitudes, and loading protocols. They discovered that SMA rebars exhibit excellent and stable flag-shaped hysteretic loops under tension-compression loadings, and that loading frequency had a negligible effect on the equivalent viscous damping. Figure 13 presents the behavior of the Ni-Ti SMA subjected to tension-compression loading with varying loading frequencies. As can be seen, the behavior of the rebar under the load with a frequency of 0.01 Hz overlapped the behavior of the rebar under quasi-static loading. It is also clear that the loading frequency had a significant influence on the hysteretic curve in the compressive direction. Generally, loading frequency did not affect the forward transformation stress of the rebar, while the absolute value for reverse transformation stress decreased in tension and compression when loading frequency increased. The difference between curves under loading with different frequencies was due to an increase in surface temperature under high frequency. However, loading frequency did not influence the residual strain.

SMA rebar. Figure 11 compares the cyclic behavior of a 7.1 mm SMA rod under cyclic loading at different frequencies. It is evident from Figure 11 that a rise in loading frequency reduces the area of the hysteresis loops and, hence, the dissipated energy. Therefore, it is anticipated that the effect of loading frequency on the mechanical properties of SMAs will be significant, particularly when the structure is subjected to seismic loading. McCormick et al. (2007) found that an earthquake loading with non-uniform cycles had no impact on cyclic properties compared to cyclic tensile tests conducted at similar rates on full-scale specimens. Figure 12 compares the hysteresis curve for 12.7 mm Ni-Ti SMA rebar under cyclic loading and earthquake loading. As shown, the hysteresis curve for the Ni-Ti SMA rebar under cyclic loading is in the same range as that under the earthquake loading.

Until now, few research has examined the cyclic behavior of Ni-Ti SMA bars under tension-compression loads. Wang and Zhu (2018) examined the cyclic behavior of a Ni-Ti SMA rebar with buckling restrained devices (BRDs) under tension-compression cyclic loadings in an experimental study. The behavior of SMA rebars was assessed under loadings with

Several researchers have studied the cyclic behavior of Cu-SMAs in recent years due to their cost effectiveness and comparable superelastic strain recovery compared to Ni-Ti SMAs. Zhang et al. (2009) experimentally studied the mechanical properties of 1.4 mm Cu-Al-Be alloy wires at different temperatures (−50°C, −25°C, 0°C, and 50°C) and loading rates. The results showed that loading frequency has a little effect on the mechanical properties, and Cu-Al-Be alloy wires demonstrated superelastic behavior at different temperatures. Figure 14(a) illustrates the effects of temperature on the stress-strain curve. Although the transformation plateau stress decreased when the temperature decreased, the elastic modulus remained constant. Hong et al. (2022) examined the fatigue behavior of 20 mm Cu-Al-Mn SMA rebar at three different temperatures (−40°C, 25°C, and 50°C) under a tensile strain amplitude of 5%. The results showed that the superelastic behavior of Cu-Al-Mn rebar is not
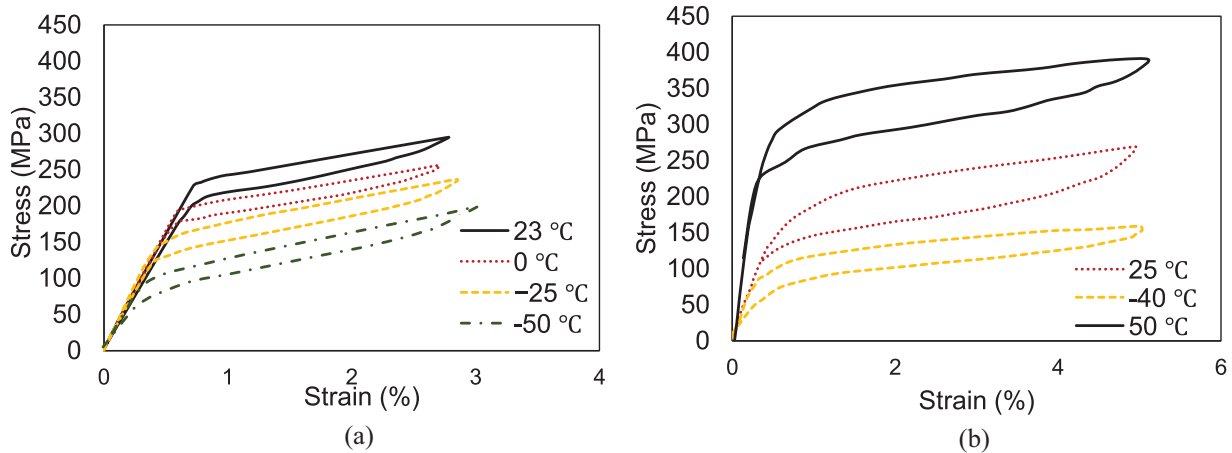
Figure 14. Temperature effect on the behavior of Cu SMA: (a) Cu-Al-Be SMA (Zhang et al., 2009) and (b) Cu-Al-Mn SMA (Hong et al., 2022).
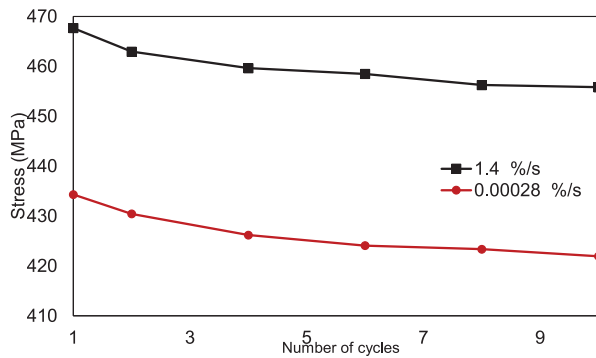

Figure 15. Effect of cyclic loading with different rates on the maximum stress of Fe SMA (Rosa et al., 2021).

sensitive to the temperature, and in all three temperatures, the superelastic behavior of rebar can be observed. Figure 14(b) compares the stress-strain curve of the Cu-Al-Mn SMA at different temperatures. According to this figure, when the temperature is increased, the transformation plateau stress increased.

Furthermore, Ghafoori et al. (2017) experimentally assessed the cyclic and fatigue behavior of Fe-SMA (Fe-17Mn-5Si-10Cr-4Ni-1(V,C)) strips having thickness of 1.5 mm and width of 100 mm. Cyclic tensile tests with two different strain rates were performed on five pre-strained and pre-heated samples to characterize the mechanical properties and recovery strain of the Fe-SMAs. It was observed that loading rate affects the mechanical properties of Fe-SMA. The specimens under high strain rates showed higher stress levels than the specimens under low strain rates due to the stress relaxation caused by the slow loading rate. Figure 15 shows the effects of loading rate on the maximum stress of the rebar and it is shown that when the strain rate decreased from 1.4%/s to 0.00028%/s the maximum stress decreased by about 10%. Rosa et al. (2021) conducted an experimental study to evaluate the behavior

of Fe-SMA round bar with the diameter of 12 mm (the diameter of reduced section is 6 mm) under tension-compression cyclic loading with different frequencies and at different temperatures. They also studied the effects of strain loading rate on the surface temperature of the rebar, which can influence the phase of transformation of the Fe-SMA rebar. They found that the loading rate between $0.03\%/s$ and $0.8\%/s$ does not have a significant effect on the surface temperature, while an increase of 75°C can be observed on the temperature of the specimens when exposed to the cyclic load with the strain rate of 8%/s, which is expected during the earthquake loading. Therefore, the stress-temperature phase of the diagram is important to understand the behavior of SMAs in different temperature. In an experimental study, Lee et al. (2013b) examined the phase transformation behavior of Fe–Mn–Si–Cr–Ni–1(V,C) SMAs under uniaxial tensile loading at different temperatures. The results revealed that the reverse transformation occurs when the temperature is within 0°C–175°C, and with an increase in stress level, the transformation temperature increases. It is also found that the start transformation loading stress initially increases and then decreases when the temperature increases. However, this study has been conducted under tensile loading, and it is required to find the behavior of Fe SMA under tensile-compressive loading at different temperatures. A summary of the effects of temperature and loading frequency on different compositions of SMAs is presented in Table 4.

6.3. Effect of diameter

Various diameters of SMA rebars and wires have been utilized in various civil engineering applications. Therefore, it would be essential to comprehend the precise effect of various diameters on the stress-strain

Table 4. A summary of the effects of temperature and loading frequency on different compositions of SMAs.

Compositions	Temperature	Loading frequency	Ref
Ni-Ti	• The temperature affected residual strain. • The hysteretic loop is affected by temperature. • A rise in temperature caused an upward movement of the hysteretic curve. • An increase in the temperature caused the area of the hysteretic loop and dissipated energy to decrease.	• Loading frequency did not affect the residual strain. • An increase in loading frequencies decreased the area of the hysteretic loop and, as a result, the dissipated energy. • A rise in strain loading rate decreased the equivalent damping.	DesRoches et al. (2004), McCormick et al. (2007), Wolons et al. (1998)
Cu-Al-Be	• The alloy showed superelastic behavior at different temperatures. • A rise in temperatures increased the transformation plateau stress. • The modulus of elasticity was not dependent on the temperature.	• Loading frequency had a little impact on the mechanical properties.	Zhang et al. (2009)
Cu-Al-Mn	• The alloy showed superelastic behavior at different temperatures. • A rise in temperature increased the modulus of elasticity. • A rise in temperature increased start transformation stress.		Hong et al. (2022)
Fe–Mn–Si–Cr–Ni–1(V,C)	• The reverse transformation occurred when the temperature is between $0°C - 150°C$, and with an increase in stress level, the transformation temperature increases	• Loading frequency affected the mechanical properties of alloys. • A rise in loading frequency increased the stress level. • A rise in loading frequency increased the surface temperature of the alloys.	Ghafoori et al. (2017), Lee et al. (2013b), Rosa et al. (2021)

response of SMA wires and bars. This section discusses diameter effect on the cyclic properties of SMAs.

According to previous research, there is a lack of information regarding the superelastic behavior of large diameter SMA rebars. DesRoches et al. (2004) investigated the behavior of superelastic Ni-Ti SMA rebars with varying diameters under cyclic tensile loadings. In this investigation, the performance of SMA wires with a diameter of 1.8 mm and rebars with a diameter of 25.4 mm was compared under cyclic loading to determine the effects of rebar size on the damping, strength, and recentering behavior of Ni-Ti SMAs. The results demonstrated that SMA wires exhibit greater tensile strength and damping characteristics than SMA rebars. In addition, it was discovered that section size has no effect on the recentering capabilities based on residual strains. It is also noteworthy that both SMA wires and rebars demonstrated low damping potential. McCormick et al. (2007) evaluated the behavior of Ni-Ti SMA rebars with 31.75, 19.1, and 12.7 mm diameters subjected to cyclic tensile loadings. To prevent stress concentration at grips, the diameter of these rebars was reduced to 25, 12, and 6.35 mm, respectively, at their gage lengths. While the recentering capacity and equivalent viscous damping values increased as bar size decreased, the initial modulus of
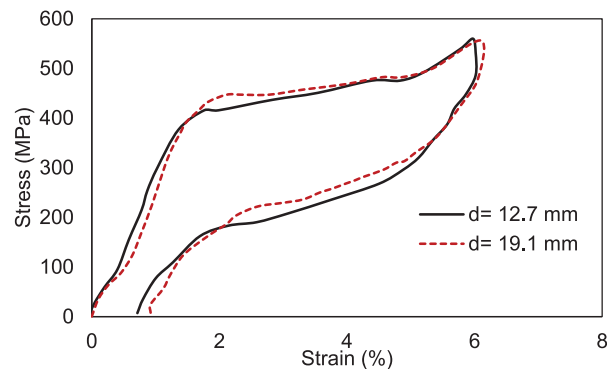

Figure 16. The hysteresis curve for the rebars with the diameters of 19.1 mm (12.7 mm reduced) and 12.7 mm (6.35 mm reduced) (McCormick et al., 2007).

elasticity and residual strain were greater for the larger-sized rebars. Under cyclic loading, all diameters of reinforcing bars demonstrated ideal superelastic behavior. Figure 16 depicts the stress-strain curve for rebars with diameters of 19.1 and 12.7 mm.

Araki et al. (2011) evaluated the cyclic behavior of 4- and 8-mm Cu-Al-Mn SMA rebars subjected to quasi-static tensile loading. They found that Cu-Al-Mn SMA rebars with diameters of 4 and 8 mm have approximately
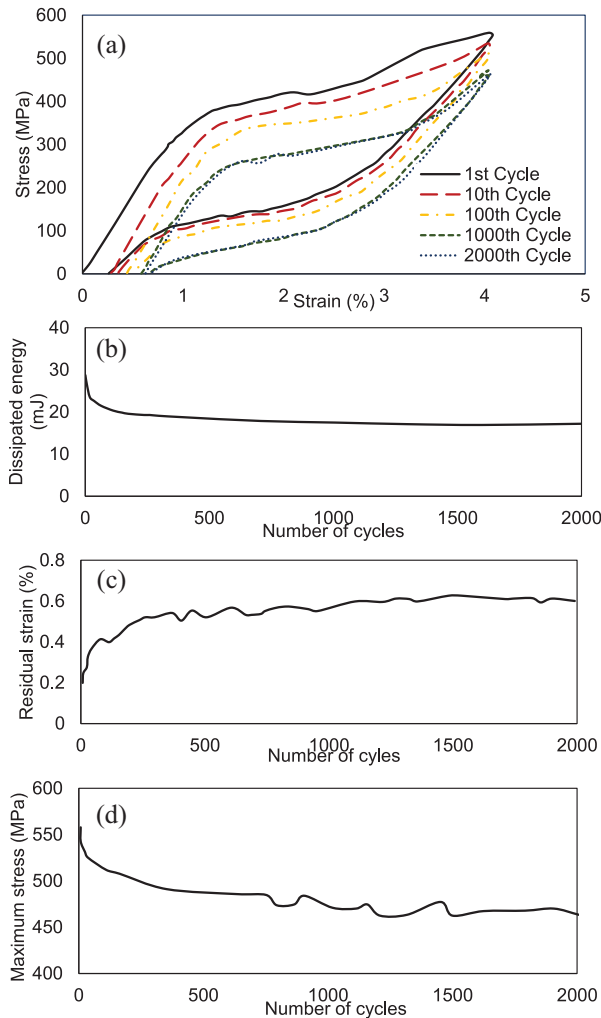
Figure 17. The LCF behavior of a Ni-Ti SMA strand at strain amplitude of 4%: (a) stress-strain curves, (b) dissipated energy versus the cycle number, (c) residual strain versus the cycle number, and (d) maximum stress versus the cycle number (Yang et al., 2021).

12% and 9% recovery strain, respectively. Depending on the strain amplitude, the equivalent damping ratio of the SMA rebar with a diameter of 8 mm increased from 2% to 7%. To evaluate the effects of section size on the cyclic properties of Cu-Al-Mn SMA rebars, they concluded that additional research is required.

6.4. Low cycle fatigue (LCF) effects

During seismic events, seismic design codes permit concrete elements to undergo significant inelastic deformation in particular regions, referred to as "plastic hinge zones." Consequently, the reinforcing rebar located in these regions undergoes large inelastic strain reversals (tension and compression) when resisting seismically induced forces, leading to the accumulation of LCF damage in the rebars (Tripathi et al., 2018). LCF is defined as the fracture of a rebar under a number of loading cycles less than 10^5 (Stephens et al., 2000). Over the lifespan of a structure (buildings, bridges), fatigue damage can develop in reinforcing bars as a result of a series of events, such as moderate to severe ground motion, and cause premature fractures (Tripathi et al., 2018). When rebars in RC structures fail due to fatigue, the structure's performance is reduced, and it may collapse. They are unable to perform their intended functions and may result in structural failure (Tripathi et al., 2018). Therefore, many research have been conducted focusing on the LCF behavior of reinforcing rebars (Brown and Kunnath, 2004; Hawileh et al., 2010; Mander et al., 1994).

Although a number of studies have focused on the LCF behavior of various types of reinforcing steel rebar (HSS, stainless, and others), very few studies have been conducted on the LCF behavior of various SMA compositions (Maletta et al., 2014; Sherif and Ozbulut, 2018; Yang et al., 2021). Due to their applications in civil engineering and seismic control devices, the LCF behavior of superelastic SMAs is important. Past studies (Liu et al., 2021; Sgambitterra et al., 2019; Wang et al., 2022) showed that SMA rebars and bolts might experience fracture when being under tensile cyclic loadings. Maletta et al. (2014) investigated the LCF behavior of commercial pseudoelastic Ni-Ti alloy sheets with the thickness of 1.5 mm subjected to various strain amplitudes. The results demonstrated that as the number of cycles increased, the energy dissipated in each cycle decreased due to a reduction in the area of the stress-strain loop, with the decline being greater for larger strain amplitudes. It is also discovered that the residual strain of pseudo-elastic Ni-Ti alloy sheets increases as the number of cycles increases. Yang et al. (2021) experimentally investigated the effects of LCF on a Ni-Ti SMA strand consisting with seven wires (diameter = 0.19 mm)subjected to varying strain amplitudes. Figure 17 shows the fatigue behavior of the Ni-Ti strand. Figure 17(a) demonstrates that as the number of cycles increased, the plateau decreased and the hysteresis loop got smaller. Thus, the amount of dissipated energy decreased. Figure 17(b) illustrates the variations in the amount of energy dissipated per cycle. Figure 17(a) and (c) also demonstrate that the amount of residual strain increased as the number of cycles increased. However, the maximum stress level decreased.

Hong et al. (2022) investigated the fatigue performance of Cu-Al-Mn SMAs at various temperatures. Figure 18 shows the stress-strain curve of Cu-SMA rebar at different cycles. As shown, the hysteretic loop became smaller when the number of loading cycles increased and consequently the dissipated energy decreased. During the first 100 cycles, the stress-strain curve displayed an ideal flag shape, indicating constant energy dissipation and strain recovery. From 100 to 1000 cycles, however, a reduction in these capacities
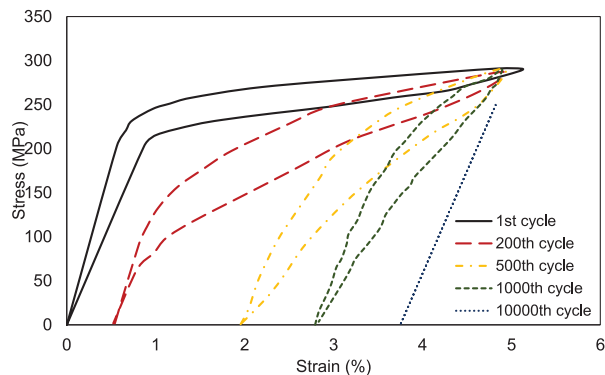
Figure 18. Cyclic stress-strain behavior of Cu SMAs (Hong et al., 2022).

was observed. After 3000 cycles, the hysteretic curves became a line, and the damping coefficient reached zero. Cu-Al-Mn SMA rebar also showed good fatigue life at different temperatures. Therefore, due to their slow degradation in mechanical properties, insensitivity to ambient temperatures, and long fatigue life at low cycles, Cu-Al-Mn SEAs are suitable for seismic applications in different climate conditions. Zhang et al. (2009) found that when temperature decreases, the fatigue life of Cu-Al-Be SMA wires increases.

Ghafoori et al. (2017) concluded that Fe-SMA demonstrated a desirable fatigue behavior under cyclic loading since the rebar did not fracture after 2,000,000 loading cycles. It should be noted that after these numbers of cycles, the rebar loses 10%–20% of its activation stress, so this loss should be considered in the design of structures.

Fang et al. (2021) evaluated the behavior of Fe-SMA under monotonic and tension-compression cyclic loadings to evaluate its suitability for seismic applications. The results revealed that Fe-SMA shows good ductility up to the fracture strain of 55%, and the hysteretic curve of Fe-SMA is stable and symmetric. The superelasticity of the Fe-SMA causes its hysteretic curve to be narrower with more hardening than that of mild steel. They also assessed the LCF behavior of Fe-SMA and concluded that Fe-SMA demonstrated better fatigue

behavior than other steels. For a strain amplitude of 1%–9%, the number of cycles to failure varies from 4007 to 83.

As stated, the fatigue life of a structural element is determined by the number of cycles at which it fails. The fatigue life for different compositions of SMAs and steel is compared in Table 5. According to the table, SMAs presented a more desirable fatigue life in comparison with the mild steel and the stainless steel. Therefore, it would be more appropriate to use it in seismic applications, in which the element undergoes high frequency cyclic loading.

Furthermore, Maletta et al. (2014) and Fang et al. (2021) developed a correlation between strain amplitude and the number of half cycles for pseudo-elastic Ni-Ti SMA alloys and Fe SMAs, respectively, using the Basquin-Coffin-Manson relationship to predict the fatigue life at different strain amplitudes. Several researchers have proposed fatigue life prediction to predict the number of cycles that a structural element can withstand under cyclic loading (Aldabagh and Alam, 2021; Brown and Kunnath, 2004; Hawileh et al., 2010; Kashani et al., 2015b; Mander et al., 1994; Tripathi et al., 2018). In the literature, the fatigue life prediction model is calculated in terms of, plastic strain, total strain amplitude, and dissipated energy (Tripathi et al., 2018). Strain-based fatigue life models, such as the total strain and plastic strain amplitude (ε_{ap}), are commonly used because they are easy to implement in FE analysis software. Coffin (1954) and Manson (1953) provided a general definition for the fatigue life model that is represented as follows:

$$\varepsilon_a = \varepsilon_{elastic} + \varepsilon_{plastic} = \frac{\sigma'_f}{E}(2N_f)^b + \varepsilon'_f(2N_f)^c \quad (1)$$

Where ε_a is total strain, $\varepsilon_{elastic}$ is elastic strain, $\varepsilon_{plastic}$ is plastic strain, σ'_f is yield stress, E is elastic modulus, $2N_f$ is the number of half cycle, b, c, and ε'_f, are the constants of fatigue life to be calibrated from experiments.

Coffin (1954) and Manson (1953) developed the fatigue life model of a metal using the relationship between ε_{ap} and the $2N_f$. The proposed LCF is represented as follows:

Table 5. A comparison for the fatigue life of SMAs and Steels.

Material	Type	Strain amplitude	1%	2%	3%	5%	Reference
		Dimension (mm)	N	N	N	N	
Ni-Ti SMA	Strand	$d = 0.57$	92,207	18,597	—	—	Yang et al. (2021)
Ni-Ti SMA	Sheet	$w = 3.5$, $t = 1.5$	3384	784	560	—	Maletta et al. (2014)
Fe-SMA	Rebar	$d = 15$	4007	—	880	—	Fang et al. (2021)
Cu-SMA	Rebar	$d = 12.7$	—	—	—	7000–50,000	Hong et al. (2022)
Q235 mild steel	Rebar	—	578	—	35	—	Fang et al. (2021)
Stainless steel	Rebar	$d = 14$ mm	159–175	23–24	6	—	Li et al. (2022)

d: diameter; *w*: width; *t*: thickness; *n*: number of cycles.

$$\varepsilon_{ap} = \varepsilon_f' \left(2N_f\right)^c \qquad (2)$$

Where ε_{ap} is plastic strain amplitude.

Furthermore, as it would be difficult to determine the precise ε_{ap} from the experimental test outcomes, Koh and Stephens (1991) developed the LCF model presented by Coffin Jr, Schenectady, and Manson. Since Koh and Stephens (1991) concluded that for the majority of fatigue analysis problems, the elastic strain remains constant, it can be neglected. As a result, total strain amplitude (ε_a) can be considered in developing a fatigue life model. Equation (3) presents the model developed by Koh and Stephens (1991).

$$\varepsilon_a = \beta \left(2N_f\right)^a \qquad (3)$$

Where the fatigue ductility coefficient is represented by β and the fatigue ductility exponent is represented by a, that can be calibrated with experimental results, and $2N_f$ is the number of half cycles till failure occurs.

As discussed, several researchers studied the LCF behavior of rebars (Brown and Kunnath, 2004; Hawileh et al., 2010; Mander et al., 1994) and developed a relationship to predict the fatigue life behavior of rebars. However, they found that rebar buckling is one of the most critical and common failure modes observed during the tests on RC structures and earthquakes in the past. Most of the RC structures that were damaged had buckled reinforcing bars. As a result, several researchers evaluated the LCF behavior of reinforcing steel rebar considering the effects of inelastic buckling and developed an equation to estimate the fatigue life of rebars based on strain amplitude and slenderness (Aldabagh and Alam, 2021; Kashani et al., 2015b; Tripathi et al., 2018).

Very few study focused on the buckling behavior of SMAs under compression loading (Asfaw et al., 2020; Pereiro-Barceló and Bonet, 2017). Pereiro-Barceló and Bonet (2017) experimentally examined the instability of 12 mm Ni-Ti SMA rebar having different lengths under compressive loading. They employed rebar of different lengths to consider the effects of slenderness in their study. They found that with an increase in the slenderness ratio of the Ni-Ti SMA rebar, the effects of buckling would be considerable, and the rebar would be unstable. Asfaw et al. (2020) investigated the buckling and post-buckling behavior of 12 mm Ni-Ti SMA rebars under monotonic loading up to failure. They considered the effect of strain rate and slenderness ratio and compared the analytical critical buckling load with experimental results. They reported asymmetric tension-compression response and higher residual strain under increased loading rates. However, in the LCF evaluation of SMAs, no study considered the effect of buckling. Therefore, it is required to examine the LCF behavior of SMAs considering the buckling effects and develop an equation to predict the fatigue life of SMA rebars in terms of strain amplitude and slenderness.

It is interesting to note that there is another type of fatigue behavior, known as "functional fatigue" which can impact the behavior of SMAs. In contrast to LCF which occurs when a material is subjected to comparatively few cycles of cyclic loading prior to failure, resulting in plastic deformation and cracking, functional fatigue occurs when a shape memory material is subjected to cyclic loading with a large number of cycles, resulting in changes to the material's functional properties, such as changes to its shape recovery force or temperature (Frenzel, 2020). Since this study is focused on the low cycle fatigue behavior of SMAs, functional fatigue of SMAs have not been considered in this study. However, several studies (Nargatti and Ahankari, 2022; Shi et al., 2022; Woodworth et al., 2022) have been conducted in the past investigating the functional fatigue of SMA wires.

7. Modeling of SMAs

7.1. Constitutive models

In the literature, the structural properties of SMAs have gained great interest for investigation; nevertheless, there are no complementary computational tools to facilitate the SMA devices' design process. It is difficult to construct an effective SMA constitutive model for use in FE software, mostly due to the absence of a traditional theoretical framework and phase-dependent material responses throughout the phase of transformations (Alam et al., 2007b).

There are two approaches for modeling SMAs: phenomenology and thermodynamics. The laws of thermodynamics are combined with energy considerations in models based on thermodynamics. Despite presenting a technique to obtain exact three-dimensional constitutive rules, thermodynamics-based models are deemed difficult and computationally costly. However, phenomenological models are more useful in civil engineering applications since they can be easily transformed into FE software. This section provides an overview of various constitutive models of SMAs developed.

Since SMA wires and bars are mostly used in civil engineering applications, phenomenological models with one dimension are considered appropriate. The phenomenological models are developed using experimental tests. Several researchers proposed uniaxial phenomenological models for SMAs (Auricchio and Sacco, 1997; Auricchio et al., 1997; Auricchio and Taylor, 1997; Graesser and Cozzarelli, 1991; Ren et al., 2007; Wilde et al., 2000).

Graesser and Cozzarelli (1991) developed a one-dimensional constitutive model for SMAs. The advantages of Graesser's model include its simple formulation and consideration of the effect of loading rate on the
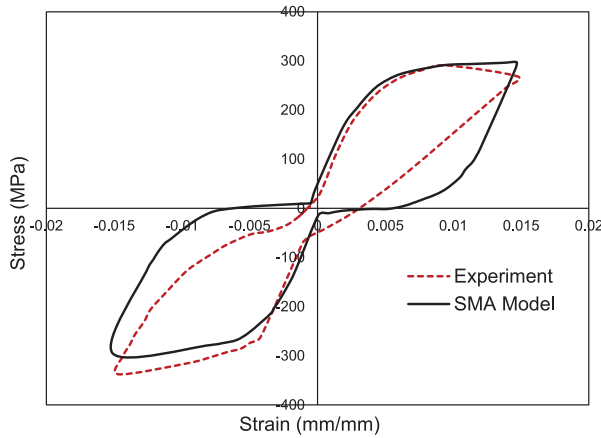
Figure 19. Comparison between the SMA stress-strain response predicted by Graesser's model and the experimental result (Graesser and Cozzarelli, 1991).

Figure 20. Hysteresis model for SMA developed by Wilde et al. (2000).

Figure 21. SMA model presented by Auricchio and Sacco (1997).

hysteretic model. However, this model was appropriate for low strain rates, and further studies were required to consider the effects of high strain rate loading on the proposed model. As discussed, a high strain loading rate is important since earthquake loading is applied with high frequency. Figure 19 compares the hysteresis responses of the proposed model and the experimental test. In Graesser's model, the behavior of material was assumed to be symmetric, while as previously discussed, the stress-strain behavior of SMAs is asymmetric, and both loading and unloading branches use identical parameters. Thus, this leads to differences between predictions and experimental results.

Wilde et al. (2000) improved the model presented by Graesser and Cozzarelli (1991). The improved model demonstrated the ability to capture SMA behavior during the transition from austenite to martensite and accurately reproduced the superelastic and shape memory behavior of SMAs. However, the model was not dependent on the temperature and the asymmetric behavior of materials was not considered. Moreover, it is difficult to extend the model to three-dimensional case. Figure 20 shows the model developed by Wilde et al. (2000).

Auricchio and Taylor (1997) developed a nonlinear model to reproduce some characteristics of SMAs, including superelastic behavior, the behavior of material in tension and compression, and single-variant-martensite reorientation processes at finite strains. The results demonstrate that the suggested model is consistent with the experimental findings. It should be noted that the thermomechanical model was not considered in the proposed model to simulate the shape memory effect.

Auricchio and Sacco (1997) developed a one-dimensional superelastic SMA model using Euler-Bernoulli beam theory. The proposed constitutive mod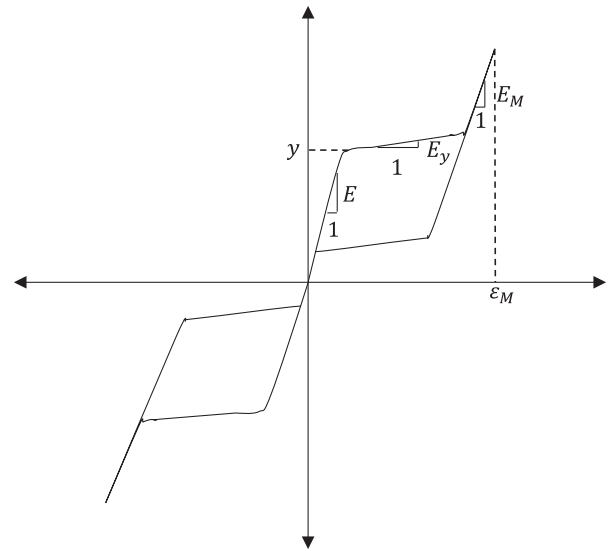el is shown in Figure 21. This model defines the material behavior in tension and compression, as well as the differences in elastic properties between austenite and martensite. This model takes into account full strain recovery and the typical flag-shaped response. The response of a beam cross section under pure bending was investigated using several numerical examples. It is concluded that SMA displays different moment-curvature relationships in tension and compression due to its unique forward and reverse transformation stress behavior.
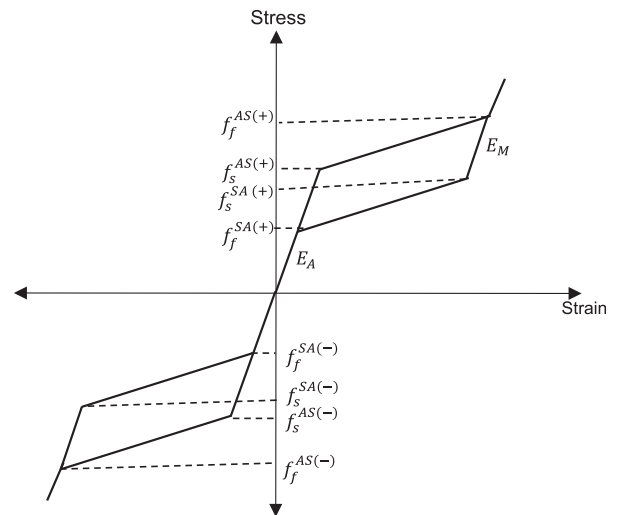
Auricchio et al. (1997) proposed a constitutive model for SMA materials in which generalized plasticity was adopted. Since the conventional model of nonlinear behavior does not provide a framework to represent shape memory and superelastic behavior, generalized
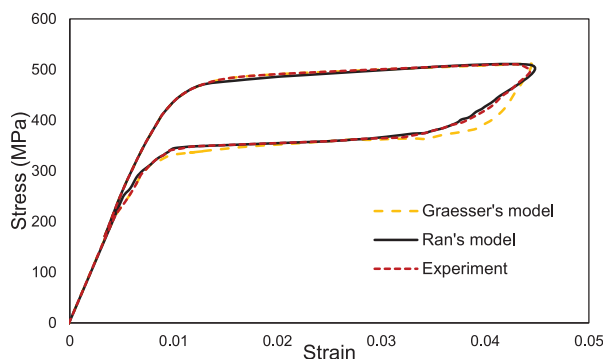
Figure 22. Comparison of the experimental response and the model developed by Ren et al. (2007).

plasticity, which has a viable and flexible behavior environment, is necessary for the development of a complex constitutive model. The proposed model can be used to assess devices with different geometries. The results showed a good match between experimental and predicted results.

Ren et al. (2007) extended Graesser and Cozzarelli's constitutive model (Graesser and Cozzarelli, 1991), in which both the loading and unloading branches use the same parameters, resulting in different predictions from experimental data to describe the superelastic behavior of SMA wires under cyclic loading. Ren et al. (2007) used different parameters during the loading and unloading branches to address the deficiency. They divided the full cycle of SMA into three parts: the loading branch, the unloading branch prior to reverse transformation, and the elastic unloading branch after reverse transformation. The results showed that the superelastic behavior of SMAs is better predicted by the Ren's model than by the original Graesser's model. Figure 22 compares the experimental and predicted superelastic behavior of 0.8 mm SMA wires using Ren's and Graesser's constitutive models.

Furthermore, several researchers proposed thermo dynamics-based constitutive models of SMAs. Zak et al. (2003) compared the behavior of thermo dynamics-based models of SMAs proposed by Liang and Rogers (1997) and Brinson (1993). They found that the superelastic behavior of the SMAs using these three models is well predicted at temperatures higher than the austenite finish temperature, where the SMAs remain in the fully austenitic phase. However, at low temperatures, when the SMA is in the martensitic phase, the Brinson's model is more accurate than the other models. They also proposed a constitutive model based on Brinson's model and Auricchio's linear law of equation. It was observed that, over a wide temperature range, the behavior of the SMA is predicted more accurately than that of other models.

Ikeda et al. (2004) established a constitutive model for SMAs subjected to unidirectional loading. The

proposed model simulated the partial hysteresis loops of stress-strain-temperature relationships and showed that the model accurately depicts the measured stress-strain curve, and the results demonstrated that the model accurately represented the measured stress–strain curve.

7.2. SMA model in finite element (FE) software

SMA superelasticity has been incorporated into a number of FE programs. Figure 23 illustrates the model used in FE packages commonly used in structural engineering. Table 6 summarizes the properties and parameters of the constitutive model used by different FE software to simulate SMA superelastic behavior. The superelasticity model provided in ABAQUS and LS-DYNA is based on the study of Auricchio and Sacco (1997) and Auricchio and Taylor (1997). The proposed model reproduced the characteristics of superelastic behavior, different material behavior in tension and compression, and the single-variant martensite reorientation process for SMAs. Figure 23(a) and (b) show the models used in ABAQUS and LS-DYNA, respectively. The superelastic model is characterized based on the uniaxial stress-strain response of the transformation phase. As discussed previously, the stress-strain behavior of some compositions of SMAs is asymmetric, and the model presented in both software packages can consider the asymmetric behavior of SMAs. In ABAQUS, the parameter of σ_{cl}^S (Austenite-to-martensite starting stress) should be defined to consider the asymmetric behavior of SMAs, but in LS-DYNA, the parameter α, which is defined as the difference between the tensile and compressive behavior of SMAs can be considered. The model presented in both FE packages also considers the difference between the modulus of elasticity in the austenite and martensite phases.

OpenSees and SeismoStruct model the superelastic behavior of SMAs using the model proposed by Fugazza (2003) (Figure 23(c) and (d)). This model is a modification of Auricchio and Sacco (1997) and can be used to describe the behavior of materials under arbitrary loads, where the response consists primarily of sub-hysteresis loops linked with complete phase transformations. It is assumed that cyclic loading has no effect on the material's strength and that the austenite and martensite branches have the same modulus of elasticity. This model also considers the material behavior to be symmetric, therefore the material response is the same in both tension and compression region.

According to past experimental studies (DesRoches et al., 2004; Hong et al., 2022; Wang and Zhu, 2018), it has been shown that SMAs experience small residual strain under cyclic loading despite their good superelastic behavior. This residual strain happens when planes of densely packed atoms glide past one another; individual bonds are broken and rebuilt with fresh atoms.
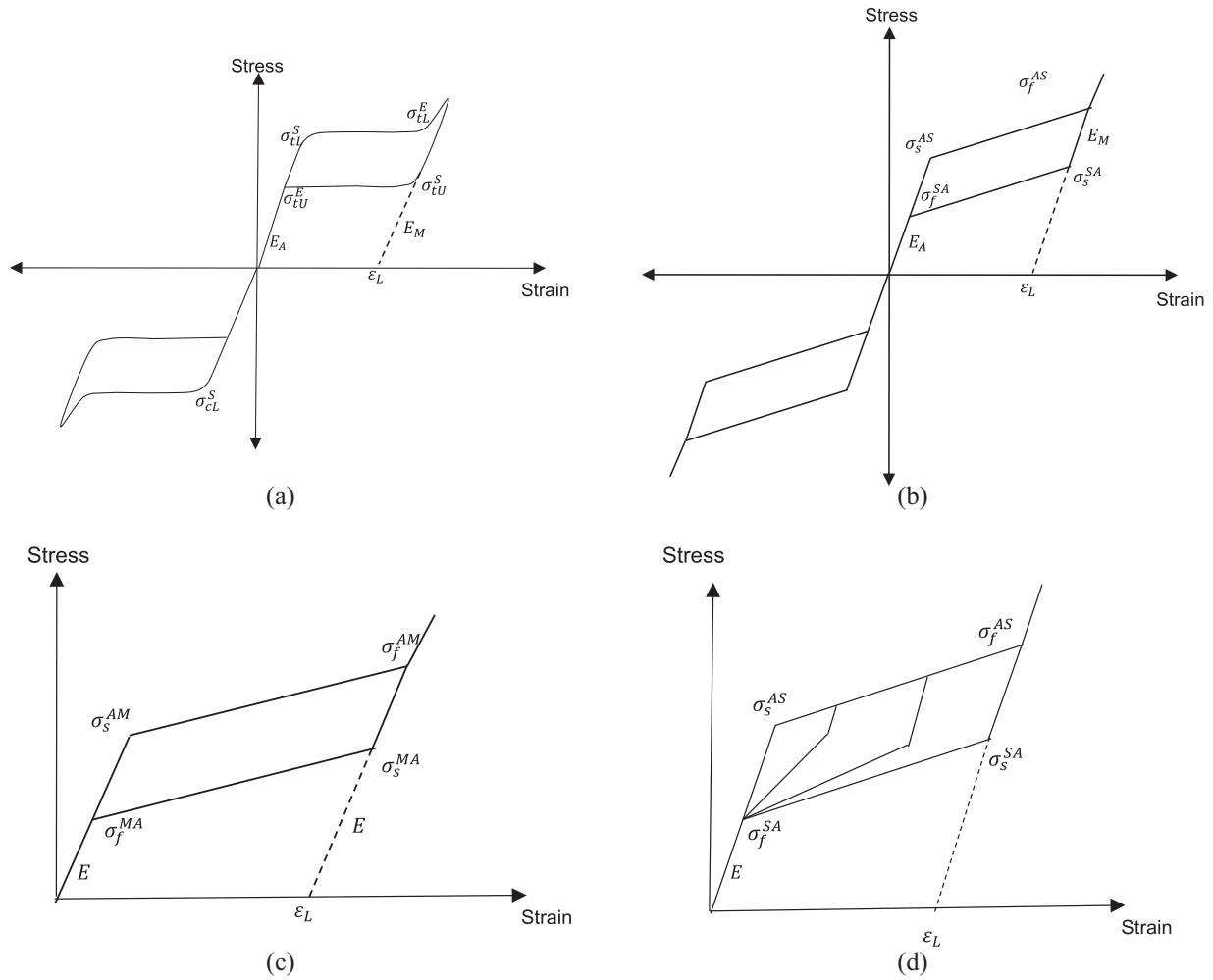
Figure 23. Constitutive models used in FE packages: (a) ABAQUS, (b) LS-DYNA, (c) OpenSees, and (d) SeismoStruct.

Table 6. SMA models used in finite element software.

Software	Parameters	Features	Reference
ABAQUS	E_A, E_M, ε_l, σ_{tl}^s, σ_{tl}^f, σ_{tu}^s, σ_{tu}^f, σ_{cl}^s	- The temperature effect is considered. - The effect of loading frequency is considered. - The asymmetric behavior of SMAs is considered - The effect of buckling is not considered	Abaqus (2011)
LS-DYNA	E_A, E_M, ε_l, σ_s^{AS}, σ_f^{AS}, σ_s^{SA}, σ_f^{SA}, α	- The effect of strain rate is considered. - The asymmetric behavior of SMAs is considered. - The effect of temperature is not considered. - The effect of buckling is not considered	LS-DYNA (2015)
OpenSees	E, ε_l, σ_s^{AM}, σ_f^{AM}, σ_s^{MA}, σ_f^{MA}	- The material behavior is assumed to be symmetric. - The model is temperature independent. - The elasticity modulus for the austenite and martensite is assumed to be constant.	Mazzoni et al. (2006)
SeismoStruct	E, ε_l, σ_s^{AS}, σ_f^{AS}, σ_s^{SA}, σ_f^{SA}	- The model is rate independent. - The model is temperature independent. - The model assumes constant modulus of elasticity for the austenite and martensite phases. - The effect of buckling is not considered.	Seismosoft (2022)

$E = E_A$: austenite modulus of elasticity; E_M: martensite modulus of elasticity; ε_l: uniaxial transformation strain; $\sigma_{tl}^s = \sigma_s^{AM} = \sigma_s^{AS}$: austenite-to-martensite starting stress (tension); $\sigma_{tl}^f = \sigma_f^{AM} = \sigma_f^{AS}$: austenite-to-martensite finishing stress (tension); $\sigma_{tu}^s = \sigma_s^{MA} = \sigma_s^{SA}$: martensite-to-austenite starting stress (tension); $\sigma_{tu}^f = \sigma_f^{MA} = \sigma_f^{SA}$: martensite-to-austenite finishing stress (tension); σ_{cl}^s: austenite-to-martensite starting stress (compression); α: a parameter that measures the difference between the tension and compression responses of a material.
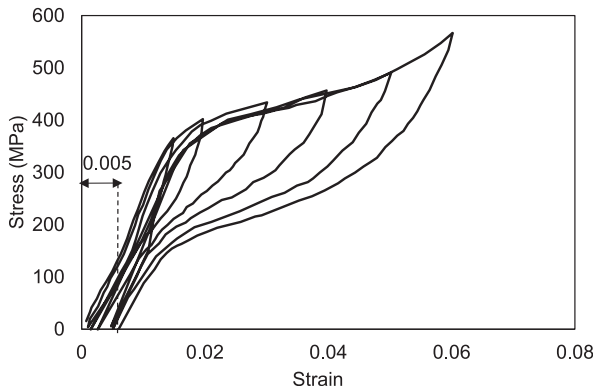
Figure 24. Cyclic behavior of Ni-Ti SMA rebar with the diameter of 25.4 mm under the tensile loading (DesRoches et al., 2004).

Figure 25. Validation of the SMA model developed by Haque and Alam (2017).

Figure 26. The stress-strain response of NiTi SMA rebar with different slenderness under compression loading (Pereiro-Barceló and Bonet, 2017).

These residual deformations accumulate and depart from the expected zero residual strain flag-shaped response under repeated cycle loading. Figure 24 shows the cyclic behavior of 25.4 mm Ni-Ti SMA rebar. As shown, the value of residual strain for the rebar is about 0.005 (0.5%) which is about 8.3% of maximum strain. Although the value of residual strain for SMAs is negligible, to represent the accurate nonlinear behavior of SMAs, it is essential to capture the residual strain (Haque and Alam, 2017). However, the models presented in FE packages are unable to capture residual strain in SMA hysteresis model. To simulate accurately SMAs' behavior under cyclic loading, Haque and Alam (2017) developed a model for SMAs in which the residual displacement of SMAs under cyclic loading can be captured. This material model was implemented in a Matlab-based FE software, and the findings indicated that the Matlab simulation and the test result are in good agreement. Figure 25 shows the comparison of the SMA model response and the experimental result.

As previously mentioned, when a concrete member is subjected to seismic force, the buckling of reinforcing bars typically occurs at the critical zone. To forecast precisely the behavior of elements during an earthquake, it is crucial to incorporate the effects of buckling into the constitutive model of rebars. A number of researchers developed the nonlinear cyclic stress-strain relationship of steel rebars incorporating the effects of buckling (Dhakal and Maekawa, 2002; Gomes and Appleton, 1997). Gomes and Appleton (1997) modified Menegotto-Pinto's model based on the equilibrium of a plastic process occurring after instability Gomes and Appleton (1997). On the basis of a FE model, Dhakal and Maekawa (2002) also developed the Menegotto-Pinto constitutive model for steel bars that accounts for compression-induced buckling. Additionally, Massone and Moroder (2009) and Massone and López (2014) provided models for steel rebar that accounted for the effects of buckling.
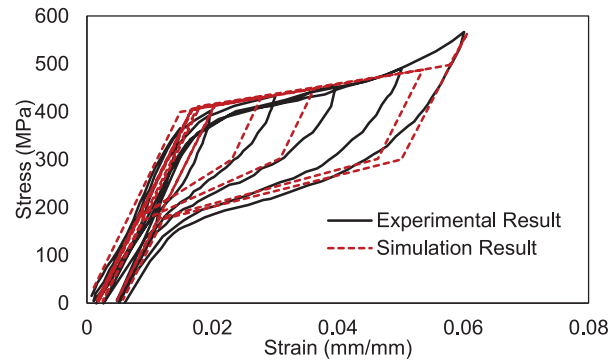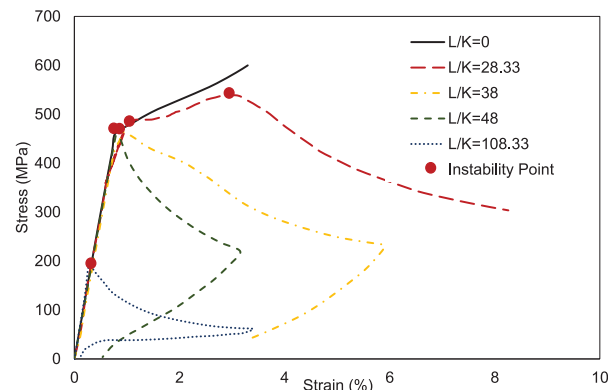
Although several studies have been done on the constitutive model for SMAs (Auricchio and Sacco, 1997; Auricchio et al., 1997; Auricchio and Taylor, 1997; Bekker and Brinson, 1998; Brinson, 1993; Fugazza, 2003; Graesser and Cozzarelli, 1991; Ren et al., 2007), very few studies have focused on the effects of inelastic buckling caused by compression (Asfaw et al., 2020; Pereiro-Barceló and Bonet, 2017). Pereiro-Barceló and Bonet (2017) examined the stability of Ni-Ti SMA rebar. Figure 26 compares the responses of the Ni-Ti rebars with different L/K slendernesses under compression-only loading. As can be seen, the slender rebars show one-instability, while the rebar with low slenderness ($L/K = 28.33$) shows two-instability points and the load can increase after the first instability. The instability points are shown with red points in Figure 26. Since the martensite transformation occurs for the rebar with low slenderness, it can be concluded that the martensite elasticity modulus is important for low slender rebar. They also developed a model in which they considered the effects of instability after buckling of the rebar based on energy equilibrium. The parametric study validated the efficiency of the proposed constitutive model. However, the suggested model did not

account for rebar's cyclic behavior under tension-compression loads. To accurately predict the stress-strain behavior of elements, it is necessary to create a constitutive model for SMAs that takes buckling into account.

8. Summary and conclusion

This paper provides an overview of the mechanical properties and cyclic behavior of various compositions of shape memory alloys (SMAs) and the factors that affect their responses. The unique characteristics of SMAs make them a suitable option for use as main reinforcement in concrete structures and core components in seismic protection devices. Several analytical and experimental studies have demonstrated that SMAs in various forms, such as rebars, wires, and plates, used in various civil engineering applications can enhance the seismic response of buildings and bridges. Additionally, the recentering capability of SMAs can be highly effective in reducing the cost of repairs after severe earthquakes. Research has also shown that the use of SMA rebars in concrete structures can decrease residual drifts caused by earthquakes compared to traditional steel rebars. To effectively utilize SMAs in seismic applications, it is crucial to understand their cyclic behavior under different conditions. This study provides a summary of the mechanical properties and cyclic behavior of SMAs so that structural engineers can accurately simulate them in finite element software. The summary of the study is as follows:

- Different compositions of SMAs have different mechanical properties (e.g. modulus of elasticity, recovery strain, and yield strength). According to past studies, Fe-Ni-Co-Al-Ta-B have high recovery strain, while the recovery strain for other compositions of SMAs is low. Cu-Al-Mn also shows a desirable recovery strain. Therefore, SMAs with a high recovery strain may be suitable for earthquake resistant applications.
- According to past studies, Ni-Ti and Cu-based SMAs show asymmetric behavior under tension-compression loading, while Fe-based SMAs exhibit a symmetric behavior. This behavior should be considered for accurate modeling of the behavior of SMAs in FE packages.
- The effects of temperature and loading rate on the cyclic behavior of SMAs are significant as they influence the area of the hysteresis loop and the amount of dissipated energy. It is interesting to note that the Cu-based SMAs are independent of loading frequency and show ideal superelastic behavior at different temperatures. So, it could be a suitable material in seismic resistance application at different temperatures.

- Many studies have been conducted on the LCF behavior of SMAs. SMAs are found to have better fatigue life behavior than other types of reinforcing steel. This proves that they can be an efficient material for seismic applications. It is noteworthy to note that when the number of cycles increases, the area of the stress-strain curve decreases, so the amount of dissipated energy decreases. However, the studies were mostly under tensile loading. Thus, the fatigue behavior of SMAs should be evaluated under tension-compression cycles to consider the effects of buckling on the fatigue behavior of SMAs.
- There are several constitutive models for SMAs, among which the models presented by Auricchio and Taylor (1997), and Auricchio and Sacco (1997) are used in different FE software. Despite the fact that the effects of buckling are important, the presented constitutive models for SMAs do not consider the effects of instability after buckling in the stress-strain behavior. This limits structural engineers to simulate the full behavior of SMAs under seismic loading. Therefore, a constitutive model should be developed for SMAs to consider the buckling effects under cyclic loading.
- Previous research has demonstrated that SMAs undergo permanent strain during cyclic loading. Although the value of residual strain is small, to accurately represent the behavior of SMAs, it is important that the SMA nonlinear model capture the residual strain under cyclic loading. However, the constitutive models presented in FE software are unable to capture the residual strain. So, in order to model the behavior of SMA accurately, a constitutive model for SMA should be developed to capture the residual strain of SMAs.

ORCID iD

AHM Muntasir Billah https://orcid.org/0000-0001-9840-3438

References

Abaqus G (2011) Abaqus 6.11. Providence, RI: Dassault Systemes Simulia Corporation.

Abdulridha A (2013) *Performance of superelastic shape memory alloy reinforced concrete elements subjected to monotonic and cyclic loading*. Doctoral Dissertation, University of Ottawa, Ottawa.

Abdulridha A and Palermo D (2017) Behaviour and modelling of hybrid SMA-steel reinforced concrete slender shear wall. *Engineering Structures* 147: 77–89.

Abraik E, El-Fitiany SF and Youssef MA (2020) Seismic performance of concrete core walls reinforced with shape memory alloy bars. *Structures* 27: 1479–1489.

Alam MS, Nehdi M and Youssef MA (2007a) Applications of shape memory alloys in earthquake engineering. In: *Proceedings of the 9th Canadian conference on earthquake engineering*, Ottawa, ON, 26–29 June, pp.26–29.

Alam MS, Youssef MA and Nehdi M (2007b) Utilizing shape memory alloys to enhance the performance and safety of civil infrastructure: A review. *Canadian Journal of Civil Engineering* 34(9): 1075–1086.

Alam MS, Youssef MA and Nehdi M (2007c) Seismic behaviour of concrete beam-column joints reinforced with superelastic shape memory alloys. In: *9th Canadian conference on earthquake engineering*, Ottawa, ON, 26–29 June 2007, p.10.

Alam MS, Youssef MA and Nehdi M (2008) Analytical prediction of the seismic behaviour of superelastic shape memory alloy reinforced concrete elements. *Engineering Structures* 30(12): 3399–3411.

Aldabagh S and Alam MS (2021) Low-cycle fatigue performance of high-strength steel reinforcing bars considering the effect of inelastic buckling. *Engineering Structures* 235: 112114.

Araki Y, Endo T, Omori T, et al. (2011) Potential of superelastic Cu-Al-Mn alloy bars for seismic applications. *Earthquake Engineering & Structural Dynamics* 40(1): 107–115.

Asfaw AM and Ozbulut OE (2021) Characterization of shape memory alloy energy dissipators for earthquake-resilient structures. *Structural Control and Health Monitoring* 28(4): e2697.

Asfaw AM, Sherif MM, Xing G, et al. (2020) Experimental investigation on buckling and post-buckling behavior of superelastic shape memory alloy bars. *Journal of Materials Engineering and Performance* 29: 3127–3140.

ASTM F2516-07 (2007) *Standard Test Method for Tension Testing of Nickel-Titanium Superelastic Materials*. West Conshohocken, PA: ASTM International.

Auricchio F and Sacco E (1997) A superelastic shape-memory-alloy beam model. *Journal of Intelligent Material Systems and Structures* 8(6): 489–501.

Auricchio F and Taylor RL (1997) Shape-memory alloys: Modelling and numerical simulations of the finite-strain superelastic behavior. *Computer Methods in Applied Mechanics and Engineering* 143(1–2): 175–194.

Auricchio F, Taylor RL and Lubliner J (1997) Shape-memory alloys: Macromodelling and numerical simulations of the superelastic behavior. *Computer Methods in Applied Mechanics and Engineering* 146(3–4): 281–312.

Ayoub CA (2003) *A study of shape-memory-alloy reinforced beams and cubes*. University of Nevada, Reno.

Bekker A and Brinson LC (1998) Phase diagram based description of the hysteresis behavior of shape memory alloys. *Acta Materialia* 46(10): 3649–3665.

Billah AM and Alam MS (2016a) Performance-based seismic design of shape memory alloy–reinforced concrete bridge piers. I: Development of performance-based damage states. *Journal of Structural Engineering* 142(12): 04016140.

Billah AM and Alam MS (2016b) Plastic hinge length of shape memory alloy (SMA) reinforced concrete bridge pier. *Engineering Structures* 117: 321–331.

Billah AM, Rahman J and Zhang Q (2022) Shape memory alloys (SMAs) for resilient bridges: A state-of-the-art review. *Structures* 37: 514–527.

Brinson LC (1993) One-dimensional constitutive behavior of shape memory alloys: Thermomechanical derivation with non-constant material functions and redefined martensite internal variable. *Journal of Intelligent Material Systems and Structures* 4(2): 229–242.

Brown J and Kunnath SK (2004) Low-cycle fatigue failure of reinforcing steel bars. *Materials Journal* 101(6): 457–466.

Buehler WJ and Wiley RC (1961) *The properties of TiNi and associated phases*. White Oak, MD: Naval Ordnance Lab.

Coffin LF Jr (1954) A study of the effects of cyclic thermal stresses on a ductile metal. *Transactions of the American Society of Mechanical Engineers* 76(6): 931–949.

Czaderski C, Shahverdi M, Brönnimann R, et al. (2014) Feasibility of iron-based shape memory alloy strips for pre-stressed strengthening of concrete structures. *Construction and Building Materials* 56: 94–105.

DesRoches R, McCormick J and Delemont M (2004) Cyclic properties of superelastic shape memory alloy wires and bars. *Journal of Structural Engineering* 130(1): 38–46.

DesRoches R and Smith B (2004) Shape memory alloys in seismic resistant design and retrofit: A critical review of their potential and limitations. *Journal of Earthquake Engineering* 8(3): 415–429.

Dhakal RP and Maekawa K (2002) Path-dependent cyclic stress–strain relationship of reinforcing bar including buckling. *Engineering Structures* 24(11): 1383–1396.

Dolce M and Cardone D (2001) Mechanical behaviour of shape memory alloys for seismic applications 2. Austenite NiTi wires subjected to tension. *International Journal of Mechanical Sciences* 43(11): 2657–2677.

Dong J, Cai CS and Okeil AM (2011) Overview of potential and existing applications of shape memory alloys in bridges. *Journal of Bridge Engineering* 16(2): 305–315.

Fang C, Wang W, Ji Y, et al. (2021) Superior low-cycle fatigue performance of iron-based SMA for seismic damping application. *Journal of Constructional Steel Research* 184: 106817.

Frenzel J (2020) On the importance of structural and functional fatigue in shape memory technology. *Shape Memory and Superelasticity* 6: 213–222.

Frick CP, Ortega AM, Tyber J, et al. (2004) Multiscale structure and properties of cast and deformation processed polycrystalline NiTi shape-memory alloys. *Metallurgical and Materials Transactions A* 35: 2013–2025.

Fugazza D (2003) *Shape-memory alloy devices in earthquake engineering: Mechanical properties, constitutive modelling and numerical simulations*. Master's Thesis, University of Pavia, Pavia, Italy.

Ghafoori E, Hosseini E, Leinenbach C, et al. (2017) Fatigue behavior of a Fe-Mn-Si shape memory alloy used for pre-stressed strengthening. *Materials & Design* 133: 349–362.

Ghassemieh M, Mostafazadeh M and Sadeh MS (2012) Seismic control of concrete shear wall using shape memory alloys. *Journal of Intelligent Material Systems and Structures* 23(5): 535–543.

Gholipour G and Billah AM (2022) Numerical investigation of shape-memory alloy–reinforced bridge columns subjected to lateral impact loads. *Journal of Bridge Engineering* 27(8): 04022063.

Gomes A and Appleton J (1997) Nonlinear cyclic stress-strain relationship of reinforcing bars including buckling. *Engineering Structures* 19(10): 822–826.

Graesser EJ and Cozzarelli FA (1991) Shape-memory alloys as new materials for aseismic isolation. *Journal of Engineering Mechanics* 117(11): 2590–2608.

Haque ABMR and Alam MS (2017) Hysteretic behaviour of a piston based self-centering (PBSC) bracing system made of superelastic SMA bars – A feasibility study. *Structures* 12: 102–114.

Hawileh RA, Abdalla JA, Oudah F, et al. (2010) Low-cycle fatigue life behaviour of BS 460B and BS B500B steel reinforcing bars. *Fatigue & Fracture of Engineering Materials & Structures* 33(7): 397–407.

Hesse T, Ghorashi M and Inman DJ (2004) Shape memory alloy in tension and compression and its application as clamping-force actuator in a bolted joint: Part 1—Experimentation. *Journal of Intelligent Material Systems and Structures* 15(8): 577–587.

Hong H, Gencturk B, Aryan H, et al. (2022) Low-cycle fatigue behavior of Cu–Al–Mn superelastic alloys at different temperatures. *Smart Materials and Structures* 31(11): 115022.

Hosseini E, Ghafoori E, Leinenbach C, et al. (2018) Stress recovery and cyclic behaviour of an Fe–Mn–Si shape memory alloy after multiple thermal activation. *Smart Materials and Structures* 27(2): 025009.

Hosseini F, Gencturk B, Lahpour S, et al. (2015) An experimental investigation of innovative bridge columns with engineered cementitious composites and Cu–Al–Mn super-elastic alloys. *Smart Materials and Structures* 24(8): 085029.

Hoult R and de Almeida JP (2022) From experimental strain and crack distributions to plastic hinge lengths of RC walls with SMA rebars. *Engineering Structures* 268: 114731.

Ikeda T, Nae FA, Naito H, et al. (2004) Constitutive model of shape memory alloys for unidirectional loading considering inner hysteresis loops. *Smart Materials and Structures* 13(4): 916–925.

Kashani MM, Alagheband P, Khan R, et al. (2015a) Impact of corrosion on low-cycle fatigue degradation of reinforcing bars with the effect of inelastic buckling. *International Journal of Fatigue* 77: 174–185.

Kashani MM, Barmi AK and Malinova VS (2015b) Influence of inelastic buckling on low-cycle fatigue degradation of reinforcing bars. *Construction and Building Materials* 94: 644–655.

Kato H, Ozu T, Hashimoto S, et al. (1999) Cyclic stress–strain response of superelastic Cu–Al–Mn alloy single crystals. *Materials Science and Engineering A* 264(1–2): 245–253.

Koh SK and Stephens RI (1991) Mean stress effects on low cycle fatigue for a high strength steel. *Fatigue & Fracture of Engineering Materials & Structures* 14(4): 413–428.

Koster M, Lee WJ, Schwarzenberger M, et al. (2015) Cyclic deformation and structural fatigue behavior of an FE–Mn–Si shape memory alloy. *Materials Science and Engineering A* 637: 29–39.

Lee WJ, Weber B, Feltrin G, et al. (2013a) Stress recovery behaviour of an Fe–Mn–Si–Cr–Ni–VC shape memory alloy used for prestressing. *Smart Materials and Structures* 22(12): 125037.

Lee WJ, Weber B, Feltrin G, et al. (2013b) Phase transformation behavior under uniaxial deformation of an Fe–Mn–Si–Cr–Ni–VC shape memory alloy. *Materials Science and Engineering A* 581: 1–7.

Lee WJ, Weber B and Leinenbach C (2015) Recovery stress formation in a restrained Fe–Mn–Si-based shape memory alloy used for prestressing or mechanical joining. *Construction and Building Materials* 95: 600–610.

Li W, Wang Q, Qu H, et al. (2022) Mechanical properties of HRB400E/316L stainless steel clad rebar under low-cycle fatigue. *Structures* 38: 292–305.

Liang C and Rogers CA (1997) One-dimensional thermomechanical constitutive relations for shape memory materials. *Journal of Intelligent Material Systems and Structures* 8(4): 285–302.

Liu W, Sun G, Chen L, et al. (2021) Experimental investigation into NiTi shape memory alloy panels under cyclic shear loading. *Engineering Structures* 245: 112958.

Liu Y, Xie Z, Van Humbeeck J, et al. (1998) Asymmetry of stress–strain curves under tension and compression for NiTi shape memory alloys. *Acta Materialia* 46(12): 4325–4338.

LS-DYNA (2015) Keyword user's manual V971. Livermore, CA: Livermore Software Technology Corporation (LSTC).

McCormick J and DesRoches R (2006) The effect of training, pre-straining, and loading history on the properties of NiTi shape memory alloys for protective systems in civil structures. In: *Structures congress 2006: Structural engineering and public safety*, pp.1–10.

McCormick J, Tyber J, DesRoches R, et al. (2007) Structural engineering with NiTi. II: Mechanical behavior and scaling. *Journal of Engineering Mechanics* 133(9): 1019–1029.

Maletta C, Sgambitterra E, Furgiuele F, et al. (2014) Fatigue properties of a pseudoelastic NiTi alloy: Strain ratcheting and hysteresis under cyclic tensile loading. *International Journal of Fatigue* 66: 78–85.

Mander JB, Panthaki FD and Kasalanati A (1994) Low-cycle fatigue behavior of reinforcing steel. *Journal of Materials in Civil Engineering* 6(4): 453–468.

Manson SS (1953) *Behavior of Materials Under Conditions of Thermal Stress*, vol. 2933. Washington, DC: National Advisory Committee for Aeronautics.

Marquis F, Kim JJ, Elwood KJ, et al. (2017) Understanding post-earthquake decisions on multi-storey concrete buildings in Christchurch, New Zealand. *Bulletin of Earthquake Engineering* 15: 731–758.

Massone LM and López EE (2014) Modeling of reinforcement global buckling in RC elements. *Engineering Structures* 59: 484–494.

Massone LM and Moroder D (2009) Buckling modeling of reinforcing bars with imperfections. *Engineering Structures* 31(3): 758–767.

Mazzoni S, McKenna F, Scott MH, et al. (2006) OpenSees command language manual. *Pacific Earthquake Engineering Research (PEER) Center* 264(1): 137–158.

Miyazaki S (1990) Thermal and stress cycling effects and fatigue properties of Ni-Ti alloys. In: Duerig TW, Melton KN, Stockel D, et al. (eds) *Engineering Aspects of Shape Memory Alloys*. London: Butterworth-Heineman, pp.394–413.

Nahar M, Billah AM, Kamal HR, et al. (2019) Numerical seismic performance evaluation of concrete beam-column joint reinforced with different super elastic shape memory alloy rebars. *Engineering Structures* 194: 161–172.

Nargatti K and Ahankari S (2022) Advances in enhancing structural and functional fatigue resistance of superelastic NiTi shape memory alloy: A review. *Journal of Intelligent Material Systems and Structures* 33(4): 503–531.

Ölander A (1932) An electrochemical investigation of solid cadmium-gold alloys. *Journal of the American Chemical Society* 54(10): 3819–3833.

Omori T, Ando K, Okano M, et al. (2011) Superelastic effect in polycrystalline ferrous alloys. *Science* 333(6038): 68–71.

Ozbulut OE, Hurlebaus S and DesRoches R (2011) Seismic response control using shape memory alloys: A review. *Journal of Intelligent Material Systems and Structures* 22(14): 1531–1549.

Paul SK, Majumdar S and Kundu S (2014) Low cycle fatigue behavior of thermo-mechanically treated rebar. *Materials & Design* 58: 402–411.

Pereiro-Barceló J and Bonet JL (2017) Ni-Ti SMA bars behaviour under compression. *Construction and Building Materials* 155: 348–362.

Rahman J and Billah AM (2020) Seismic performance evaluation of shape memory alloy (SMA) reinforced concrete bridge bents under long-duration motion. *Frontiers in Built Environment* 6: 601736.

Recarte V, Pérez-Landazábal JI, Rodrı̈guez PP, et al. (2004) Thermodynamics of thermally induced martensitic transformations in Cu–Al–Ni shape memory alloys. *Acta Materialia* 52(13): 3941–3948.

Rejzner J, Lexcellent C and Raniecki B (2002) Pseudoelastic behaviour of shape memory alloy beams under pure bending: Experiments and modelling. *International Journal of Mechanical Sciences* 44(4): 665–686.

Ren W, Li H and Song G (2007) A one-dimensional strain-rate-dependent constitutive model for superelastic shape memory alloys. *Smart Materials and Structures* 16(1): 191–197.

Rosa DIH, Hartloper A, dE Castro e Sousa A, et al. (2021) Experimental behavior of iron-based shape memory alloys under cyclic loading histories. *Construction and Building Materials* 272: 121712.

Saiidi MS, O'Brien M and Sadrossadat-Zadeh M (2009) Cyclic response of concrete bridge columns using superelastic nitinol and bendable concrete. *ACI Structural Journal* 106(1): 69–77.

Saiidi MS, Sadrossadat-Zadeh M, Ayoub C, et al. (2007) Pilot study of behavior of concrete beams reinforced with shape memory alloys. *Journal of Materials in Civil Engineering* 19(6): 454–461.

Saiidi MS and Wang H (2006) Exploratory study of seismic response of concrete columns with shape memory alloys reinforcement. *ACI Materials Journal* 103(3): 436.

Seismosoft (2022) SeismoStruct v7.0: A computer program for static and dynamic nonlinear analysis of framed structures. Available at: http://www.seismosoft.com (accessed 15 September 2023).

Sgambitterra E, Magarò P, Niccoli F, et al. (2019) Low-to-high cycle fatigue properties of a NiTi shape memory alloy. *Procedia Structural Integrity* 18: 908–913.

Shahverdi M, Michels J, Czaderski C, et al. (2018) Iron-based shape memory alloy strips for strengthening RC members: Material behavior and characterization. *Construction and Building Materials* 173: 586–599.

Sherif MM and Ozbulut OE (2018) Tensile and superelastic fatigue characterization of NiTi shape memory cables. *Smart Materials and Structures* 27(1): 015007.

Shi F, Ozbulut OE, Li Z, et al. (2022) Effects of ambient temperature on cyclic response and functional fatigue of shape memory alloy cables. *Journal of Building Engineering* 52: 104340.

Shrestha KC, Araki Y, Nagae T, et al. (2013) Feasibility of Cu–Al–Mn superelastic alloy bars as reinforcement elements in concrete beams. *Smart Materials and Structures* 22(2): 025025.

Siddiquee KN, Billah AM and Issa A (2021) Seismic collapse safety and response modification factor of concrete frame buildings reinforced with superelastic shape memory alloy (SMA) rebar. *Journal of Building Engineering* 42: 102468.

Song G, Ma N and Li HN (2006) Applications of shape memory alloys in civil structures. *Engineering Structures* 28(9): 1266–1274.

Stephens RI, Fatemi A, Stephens RR, et al. (2000) *Metal Fatigue in Engineering*. New York, NY: John Wiley & Sons.

Tanaka Y, Himuro Y, Kainuma R, et al. (2010) Ferrous polycrystalline shape-memory alloy showing huge superelasticity. *Science* 327(5972): 1488–1490.

Tazarv M and Saiid Saiidi M (2015) Reinforcing NiTi superelastic SMA for concrete structures. *Journal of Structural Engineering* 141(8): 04014197.

Tripathi M, Dhakal RP, Dashti F, et al. (2018) Low-cycle fatigue behaviour of reinforcing bars including the effect of inelastic buckling. *Construction and Building Materials* 190: 1226–1235.

Vivet A and Lexcellent C (2001) CuZnAl single crystals pseudoelastic behaviour under biaxial tensile loading: Observations and analysis. *Le Journal de Physique IV* 11(PR4): Pr4–205.

Vollmer M, Bauer A, Frenck JM, et al. (2021) Novel prestressing applications in civil engineering structures enabled by Fe Mn Al Ni shape memory alloys. *Engineering Structures* 241: 112430.

Wang B and Zhu S (2018) Cyclic tension–compression behavior of superelastic shape memory alloy bars with buckling-restrained devices. *Construction and Building Materials* 186: 103–113.

Wang W, Fang C, Ji Y, et al. (2022) Experimental and numerical studies on Fe–Mn–Si alloy dampers for enhanced low-cycle fatigue resistance. *Journal of Structural Engineering* 148(11): 04022170.

Wilde K, Gardoni P and Fujino Y (2000) Base isolation system with shape memory alloy device for elevated highway bridges. *Engineering Structures* 22(3): 222–229.

Wilson JC and Wesolowsky MJ (2005) Shape memory alloys for seismic response modification: A state-of-the-art review. *Earthquake Spectra* 21(2): 569–601.

Wolons D, Gandhi F and Malovrh B (1998) Experimental investigation of the pseudoelastic hysteresis damping characteristics of shape memory alloy wires. *Journal of Intelligent Material Systems and Structures* 9(2): 116–126.

Woodworth LA, Lohse F, Kopelmann K, et al. (2022) Development of a constitutive model considering functional fatigue and pre-stretch in shape memory alloy wires. *International Journal of Solids and Structures* 234–235: 111242.

Wu D, Ding Y, Su J, et al. (2022) Investigation on low-cycle fatigue performance of high-strength steel bars including the effect of inelastic buckling. *Engineering Structures* 272: 114974.

Yang X, Zhou H, Yang X, et al. (2021) Shape memory alloy strands as cross-ties: Fatigue behavior and model-cable net tests. *Engineering Structures* 245: 112828.

Youssef MA, Alam MS and Nehdi M (2008) Experimental investigation on the seismic behavior of beam-column joints reinforced with superelastic shape memory alloys. *Journal of Earthquake Engineering* 12(7): 1205–1222.

Zak AJ, Cartmell MP, Ostachowicz WM, et al. (2003) One-dimensional shape memory alloy models for use with reinforced composite structures. *Smart Materials and Structures* 12(3): 338–346.

Zhang Y, Hu X and Zhu S (2009) Seismic performance of benchmark base-isolated bridges with superelastic Cu-Al-Be restraining damping device. *Structural Control and Health Monitoring* 16(6): 668–685.

Zhao B, Taucer F and Rossetto T (2009) Field investigation on the performance of building structures during the 12 May 2008 Wenchuan earthquake in China. *Engineering Structures* 31(8): 1707–1723.